Geophysical Journal International

Geophys. J. Int. (2018) **215,** 713–735
Advance Access publication 2018 July 28
GJI Heat flow and volcanology

doi: 10.1093/gji/ggy313

Magma wagging and whirling: excitation by gas flux

Yang Liao[1] and David Bercovici[2]

[1]*Department of Geology and Geophysics, Woods Hole Oceanographic Institution, Falmouth, MA02543, Massachusetts, USA. E-mail: yliao@whoi.edu*
[2]*Department of Geology and Geophysics, Yale University, New Haven, CT02511, Connecticut, USA*

Accepted 2018 July 27. Received 2018 May 27; in original form 2018 January 25

SUMMARY

Gas flux in volcanic conduits is often associated with long-period oscillations known as seismic tremor (Lesage *et al.*; Nadeau *et al.*). In this study, we revisit and extend the 'magma wagging'and 'whirling'models for seismic tremor, in order to explore the effects of gas flux on the motion of a magma column surrounded by a permeable vesicular annulus (Jellinek & Bercovici; Bercovici *et al.*; Liao *et al.*). We find that gas flux flowing through the annulus leads to a Bernoulli effect, which causes waves on the magma column to become unstable and grow. Specifically, the Bernoulli effects are associated with torques and forces acting on the magma column, increasing its angular momentum and energy. As the displacement of the magma column becomes large due to the Bernoulli effect, frictional drag on the conduit wall decelerates the motions of the column, restoring them to small amplitude. Together, the Bernoulli effect and the damping effect contribute to a self-sustained wagging-and-whirling mechanism that help explain the longevity of long-period seismic tremor.

Key words: Physics of magma and magma bodies; Volcano seismology; Volcanic gases.

1 INTRODUCTION

1.1 Volcanic seismicity and volatile degassing

The unrest of many volcanic systems is often linked to the release of gaseous volatiles. During magma ascent, volatile exsolution and degassing are thought to induce pre-eruptive seismicity, according to both field observations and analytical models (Konstantinou & Schlindwein 2003; McNutt 2005; Lesage *et al.* 2006; Nadeau *et al.* 2011; Zuccarello *et al.* 2013). Specifically, several studies have shown that gas in the conduit can contribute to the excitation of shallow long-period seismic tremor, which is an important precursor to eruptive volcanism (Garcés *et al.* 1998; Lesage *et al.* 2006; Jellinek & Bercovici 2011; Nadeau *et al.* 2011; Bercovici *et al.* 2013). For example, waves can be excited by stirring of a magma-gas mixture and yield 1 Hz oscillations, which are often observed in volcanic tremor (Garcés *et al.* 1998). According to the 'magma wagging'model (Jellinek & Bercovici 2011), the accumulation of gas bubbles forms a vesicular annulus enveloping the magma column, allowing it to 'wag' from side to side also with a 1 Hz frequency. Bercovici *et al.* (2013) further showed that when gas flux flows through the permeable annulus, the 'wagging'motion of the magma column is excited by a Bernoulli effect, wherein pinching of the annulus causes a low pressure that enhances further pinching. In three dimensions, magma wagging can assume circular or elliptical 'whirling' motions, which possibly yield detectable spatial seismic patterns (Liao *et al.* 2018). However, in the absence of gas flux, the whirling motions are quickly damped out by viscous dissipation in the magma column. As the characteristics of the whirling motions are potentially prognostic of the intensification of volcanic unrest en route to eruption (Liao *et al.* 2018), it is important to understand how the whirling motions can be repeatedly excited, despite viscous damping. Here, we extend the above models to explore how gas flux affects the wagging and whirling motions of the magma column, especially with regard to their excitation and longevity. Our model is especially applicable to silicic volcanoes that undergo prolonged and repeated seismic tremors, including chugging events, as well as pre-eruptive degassing.

1.2 The original and extended magma wagging models

The 2-D magma wagging model developed by Jellinek & Bercovici (2011) is based on the assumption that, inside the volcanic conduit, the magma column is enveloped by a gas-rich foamy annulus. When the magma column is displaced towards one side of the conduit, the bubbles in the annulus become compressed, and their increased gas pressure pushes the magma column back towards its resting position. Because of the magma column's inertia, it overshoots the resting position, thereby triggering oscillations. When the annulus contains isolated bubbles,

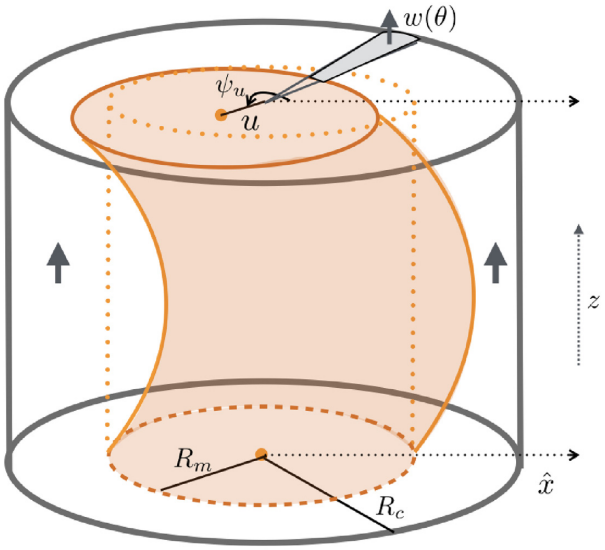

Figure 1. A sketch of the volcanic conduit (grey solid lines) and the magma column (orange shade). The amplitude u and polar angle ψ_u of the column, as well as the column's radius R_m and the conduit's radius R_c, are indicated. Black vertical arrows indicate the direction of the gas flux, whose velocity w varies with polar angle θ along the annulus. $\hat{x}$ is a basis of the Cartesian coordinates coinciding with $\theta = 0$.

the fundamental frequency for free oscillations of the magma column is

$$\omega_o = \sqrt{\frac{2\rho_o C_g^2}{\phi_o \rho_m (R_c^2 - R_m^2)}} \tag{1}$$

where ρ_o and ϕ_o are the undisturbed gas density and gas volume fraction in the annulus; C_g is the isothermal sound speed in the gas; ρ_m is the density of the magma and R_m and R_c are the radii of the magma column and the volcanic conduit, respectively (see Fig. 1). In the original study of Jellinek & Bercovici (2011), the oscillatory motions are assumed to be from side to side, without any rotational motion. Because the bubbles in the annulus are assumed to be isolated, the annulus is impermeable, thus precluding any gas flux to flow through.

The original wagging model was extended by Bercovici *et al.* (2013) to include the influence of gas flux in a permeable annulus. The authors discovered a Bernoulli-type mechanism, by which the side-to-side wagging motions can be sustained. A more recent extension of the wagging model allows for 3-D motions, in the form of 'whirling', wherein the magma column tracks elliptical trajectories, whose eccentricities depend on the energy and angular momentum of the magma column (Liao *et al.* 2018). The whirling motions also cause seismic radiation patterns spiralling away from the conduit, which are manifested as time delays between waveforms detected by seismometers at different locations. In the whirling model, the annulus is assumed to be impermeable. Lacking an excitation mechanism, the whirling motions are damped out by the viscous dissipation in the magma column. In the current study, we extend the 3-D wagging model to incorporate gas flux through a permeable annulus. We will explore if the Bernoulli effect identified in the 2-D wagging model by Bercovici *et al.* (2013) also exists in three dimensions, and whether it helps sustain the whirling motions. A theoretical framework will be presented in Section 2. Results from linear analysis, including the evolution of the magma column's angular momentum and energy will be presented in Section 3. Some non-linear effects and their influence on the motions of the magma column will be presented in Section 4, followed by discussion in Section 5.

2 THEORETICAL FRAMEWORK

2.1 Governing equations for the motion of the magma column

The geometry of our model (Fig. 1 and Fig. A1) is similar to the ones in recent studies (Bercovici *et al.* 2013; Liao *et al.* 2018), wherein a magma column, enveloped by a permeable vesicular annulus, rests in the centre of a vertical conduit. The displacement of the magma column is represented by the vector $\vec{u} = \vec{u}(z, t)$ at time t and height z along the column. In cylindrical-polar coordinates, the displacement is represented by its magnitude u, and its polar angle ψ_u, which is measured against the $\hat{x}$ unit vector in the Cartesian coordinates. The direction of $\hat{x}$, once arbitrarily selected, remains fixed for all time.

Any horizontal section of the magma column with thickness dz is subjected to a gas pressure force $\vec{F}^g$, which arises from non-uniform gas density variation in the deformed vesicular annulus surrounding the column section (see Appendix A, Fig. A1). The column section is also subjected to a viscous bending force $\vec{F}^{\rm vb}$, due to the differential shear stresses acting on its upper and lower surfaces. When the magma column moves against the annulus, the relative velocity between the moving column and the static conduit wall gives rise to a shear stress across the magma matrix in the annulus. This shear stress results in a viscous annulus drag force acting on the annulus–column interface $\vec{F}^{\rm ad}$. If the volume ratio of magma in the annulus is low, the annulus drag force $\vec{F}^{\rm ad}$ is small in comparison to the viscous bending force $\vec{F}^{\rm vb}$; hence

its effect was omitted in the previous 2-D and 3-D models (Jellinek & Bercovici 2011; Bercovici *et al.* 2013; Liao *et al.* 2018). In this study, we include $\vec{F}^{\rm ad}$, so as to study a more comprehensive coupling between the gas annulus and the magma column.

For convenience, we use grouped subscript $_{a,b,c}$ to represent the subscripts $_a$, $_b$ and $_c$ separately, and use grouped superscript ^{a,b,c} to represent ^{a}, ^{b} and ^{c} separately. According to Newton's second law, the equation of motion for the magma column section, under the three forces $\vec{F}^{g,ad,vb}$, can be expressed in Cartesian coordinates

$$\rho_m \pi R_m^2 \mathrm{d}z \frac{\partial^2 \vec{u}}{\partial t^2} = \vec{F}^g + \vec{F}^{\rm ad} + \vec{F}^{\rm vb} \tag{2}$$

When the displacement magnitude u is small compared with the width of the annulus, $u^2 < <(R_c - R_m)^2$, the three forces acting on the magma column section are, respectively (see Appendix A2)

$$\begin{aligned}
F_x^g &= -C_g^2 R_m \pi \mathrm{d}z \rho_1^c - C_g^2 \pi \mathrm{d}z \left(\rho_2^c u_x + \rho_2^s u_y\right) \\
F_y^g &= -C_g^2 R_m \pi \mathrm{d}z \rho_1^s + C_g^2 \pi \mathrm{d}z \left(\rho_2^c u_y - \rho_2^s u_x\right) \\
\vec{F}^{\rm ad} &= -\frac{\partial \vec{u}}{\partial t}(1-\phi_o)\mu_m \pi \frac{R_m}{R_c - R_m}\mathrm{d}z \\
\vec{F}^{\rm vb} &= \mu_m \pi R_m^2 \frac{\partial^3 \vec{u}}{\partial t \partial z^2}
\end{aligned} \tag{3}$$

where the subscript $_x$ and $_y$ indicate the x and y components of the given vector in the Cartesian coordinates, respectively. The isothermal sound speed for the gas phase C_g is assumed to be constant, due to the high heat capacity of the magma (Bercovici & Michaut 2010). ρ_n^c and ρ_n^s ($n = 1, 2, 3$) are the Fourier coefficients of the gas density ρ according to eq. (4), as discussed in the following section. ϕ_o is the volume fraction of the gas phase in the undeformed annulus. We assume that the magma has constant viscosity μ_m, and that the viscosity of the gas annulus is proportional to the volume fraction of magma in the deformed annulus section.

2.2 Evolution of gas density and velocity

In the permeable annulus, we assume that the sheared bubbles are tube shaped, and that the gas pathways are only in the vertical direction. Both the gas density $\rho(t, z, \theta)$ and the vertical gas velocity $w(t, z, \theta)$ are functions of time t, height z and the polar position θ along the annulus, measured against $\hat{x}$ (see Fig. A1 in Appendix A1). Given azimuthal periodicity, these functions can be expressed as discrete Fourier series

$$\begin{aligned}
\rho(\theta) &= \rho_o + \sum_{m=1}^{\infty} \left(\rho_m^c \cos m\theta + \rho_m^s \sin m\theta\right) \\
w(\theta) &= W_o + \sum_{m=1}^{\infty} \left(w_m^c \cos m\theta + w_m^s \sin m\theta\right)
\end{aligned} \tag{4}$$

in which the Fourier coefficients ρ_n^c, ρ_n^s, w_n^c and w_n^s are functions of t and z. ρ_o and W_o are the unperturbed gas density and velocity in the steady state.

The evolutions of ρ and w are coupled to each other, and can be found via conservation of mass and momentum in both the gas phase and magma matrix in the annulus, following Bercovici *et al.* (2013) (see Appendix A3)

$$\frac{\partial(\rho\varphi)}{\partial t} + \frac{\partial(\rho\varphi w)}{\partial z} = 0 \tag{5a}$$

$$\rho\phi\left(\frac{\partial w}{\partial t} + w\frac{\partial w}{\partial z}\right) = -C_g^2 \frac{\partial \rho}{\partial z} - ((1-\phi)\rho_m + \phi\rho)\, g \tag{5b}$$

where g is the gravitational acceleration, and (see Appendix A3)

$$\varphi(\theta) = \phi_o - \left(\frac{u_x}{U_m}\cos\theta + \frac{u_y}{U_m}\sin\theta\right) \tag{6a}$$

$$\phi(\theta) = \phi_o - (1-\phi_o)\left(\frac{u_x}{U_m}\cos\theta + \frac{u_y}{U_m}\sin\theta\right) \tag{6b}$$

where $U_m \equiv \frac{R_c^2 - R_m^2}{2R_m}$. We can obtain the evolution equations for the Fourier coefficients by substituting eq. (4) into the governing eq. (5). Therefore, the evolution of the system, including the magma column and the gas flux, is determined by eqs (2) and (5).

3 EVOLUTION OF THE SYSTEM WITH SMALL PERTURBATIONS

3.1 Linear stability analysis

We select the width of the annulus $R_c - R_m$ for the length scale, $(R_c - R_m)/C_g$ for the timescale, the unperturbed gas density ρ_o for the density scale and non-dimensionalize the governing eqs (2) and (5). The resulting dimensionless evolution equations are

$$\frac{\partial(\rho\varphi)}{\partial t} + \frac{\partial(\rho\varphi w)}{\partial z} = 0 \tag{7a}$$

$$\rho\phi\left(\frac{\partial w}{\partial t} + w\frac{\partial w}{\partial z}\right) = -\frac{\partial \rho}{\partial z} - \gamma\left(\beta(1-\phi) + \rho\phi\right) \tag{7b}$$

$$\frac{\partial^2 u_x}{\partial t^2} = -\frac{\lambda}{\beta}\rho_1^c - \frac{\lambda^2}{\beta}(\rho_2^c u_x + \rho_2^s u_y) + \eta\frac{\partial^3 u_x}{\partial z^2 \partial t} - (1-\phi_o)\eta\lambda\frac{\partial u_x}{\partial t} \tag{7c}$$

$$\frac{\partial^2 u_y}{\partial t^2} = -\frac{\lambda}{\beta}\rho_1^s + \frac{\lambda^2}{\beta}(\rho_2^c u_y - \rho_2^s u_x) + \eta\frac{\partial^3 u_y}{\partial z^2 \partial t} - (1-\phi_o)\eta\lambda\frac{\partial u_y}{\partial t} \tag{7d}$$

where ρ, w, and $u_{x,y}$ have been normalized by their respective scales. The dimensionless constants are defined as

$$\beta = \rho_m/\rho_o, \quad \lambda = \frac{R_c - R_m}{R_m}, \quad \eta = \frac{\mu_m}{\rho_m C_g (R_c - R_m)}, \quad \gamma = \frac{(R_c - R_m)g}{C_g^2} \tag{8}$$

where the dimensionless number β is the ratio of magma and gas density, λ is a measure of annulus thickness relative to the column width, η measures the competition between the viscous bending forces and gas spring forces and γ represents the ratio of hydrostatic pressure and gas pressure.

Using linear perturbation theory and assuming $g = \gamma = 0$ following Bercovici *et al.* (2013), we obtain the governing equations for small perturbations (see Appendix B1)

$$(\frac{\partial}{\partial t} + M\frac{\partial}{\partial z})(\phi_o\rho_1^{c,s} - \zeta u_{x,y}) + \phi_o\frac{\partial w_1^{c,s}}{\partial z} = 0 \tag{9a}$$

$$\phi_o(\frac{\partial}{\partial t} + M\frac{\partial}{\partial z})w_1^{c,s} + \frac{\partial \rho_1^{c,s}}{\partial z} = 0 \tag{9b}$$

$$\frac{\partial^2 u_{x,y}}{\partial t^2} + \frac{\lambda}{\beta}\rho_1^{c,s} - \eta\frac{\partial^3 u_{x,y}}{\partial t \partial z^2} + (1-\phi_o)\eta\lambda\frac{\partial u_{x,y}}{\partial t} = 0 \tag{9c}$$

where $\zeta = (R_c - R_m)/U_m = 2/(\lambda + 2)$; $M = W_o/C_g$ is a gas injection Mach number, determined by the undisturbed gas flux velocity W_o. With the linear approximation, the evolution of higher degree components in gas density ρ_2^c, ρ_2^s are governed by the sound-wave equations, which are decoupled from the motion of the magma column.

Assuming all perturbations have the form e^{ikz+st}, eq. (9) leads to a relation between the complex growth rate s and wavenumber k (see Fig. B1 and Appendix B2). Similar to the findings of Bercovici *et al.* (2013), we observe that each wavenumber k corresponds to four distinct roots for s. Among the four roots, three are stable with $\mathrm{Re}(s) < 0$, indicating that the corresponding perturbations decay with time; one root is unstable with $\mathrm{Re}(s) > 0$, whose perturbations grow with time (Fig. B1a). In the 2-D model, Bercovici *et al.* (2013) recognized the unstable growing root as a consequence of the Bernoulli effect from the gas flowing through the deformable annulus, whereby the pinching/dilating in the annulus section leads to an increase/decrease in gas velocity and the associated decrease/increase in gas pressure, which causes further pinching/dilating. Similarly, the Bernoulli effect induces an instability in three dimensions as well, driving perturbations to grow in both $\hat{x}$ and $\hat{y}$ components of the displacement and serves as an excitation mechanism for 3-D whirling motions (Liao *et al.* 2018). Because of its origin, we name the unstably growing perturbations 'Bernoulli perturbations'. The perturbations in the gas density $\rho_1^{c,s}$ can be expressed as responses to the to the perturbations in the displacement $u_{x,y}$ through a complex response factor $\widetilde{\Theta}$ (see Appendix B3). Using the response factor, we express the real part of growth rate s as

$$\sigma = \frac{\mathrm{Im}(\widetilde{\Theta})\lambda}{2\omega\beta} - \frac{\eta k^2}{2} - \frac{(1-\phi_o)\lambda\eta}{2} \tag{10}$$

where $\mathrm{Im}(\widetilde{\Theta})$ is the imaginary part of the response factor, $\omega = -\mathrm{Im}(s)$ indicates the oscillation frequency of the perturbation and $\sigma = \mathrm{Re}(s)$ determines if the perturbation grows (if $\sigma > 0$) or decays (if $\sigma < 0$) with time. The first term on the right-hand side of eq. (10) suggests that the gas density response factor $\widetilde{\Theta}$ is directly linked to the growth or decay of a perturbation.

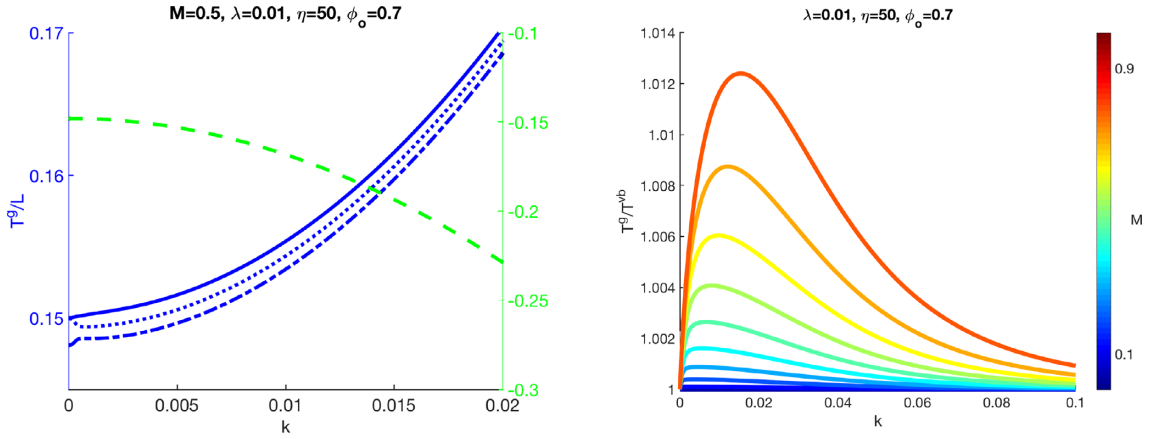

Figure 2. Frame (a) shows the magnitudes of the gas torques, normalized by the magnitude of the angular momentum according to eq. (11) as a function of wavenumber k for all roots of s [i.e. solutions for eq. (B6) in Appendix B2]. The blue curves all have positive values and correspond to the left y-axis; and the green curve has negative values and corresponds to the left y-axis. Frame (b) shows the ratio between the Bernoulli torque and the viscous bending torque as functions of k for multiple gas injection Mach numbers $M = W_o/C_g$, which are indicated by the colours of the curves.

3.2 Evolution of energy and angular momentum

3.2.1 Evolution of angular momentum under the linear forces

We define a dimensionless angular momentum $\vec{L} = \vec{u} \times \frac{\partial \vec{u}}{\partial t}$, and three dimensionless torques from the distinct linear forces $\vec{\mathcal{T}}^{g,vb,ad} \equiv \vec{u} \times \vec{F}^{g,vb,ad}$, where $\vec{F}^{\rm ad}$ and $\vec{F}^{\rm vb}$ correspond to the annulus drag and the viscous bending forces, respectively, and $\vec{F}^{g}$ corresponds to the gas pressure force due to the non-uniform linear perturbations in the gas density. For a single root with wavenumber k, angular frequency $s = \sigma - i\omega$ and gas density response factor $\widetilde{\Theta}$, the torques are related to the angular momentum as (see Appendices B5.1 and B5.2)

$$\vec{\mathcal{T}}^{\rm vb} = -\eta k^2 \vec{L}, \qquad \vec{\mathcal{T}}^{\rm ad} = -(1-\phi_o)\lambda\eta\vec{L}, \qquad \vec{\mathcal{T}}^{g} = \frac{{\rm Im}(\Theta)\lambda}{\omega\beta}\vec{L} \tag{11}$$

The torques generated by the viscous forces ($\vec{\mathcal{T}}^{\rm vb}$ and $\vec{\mathcal{T}}^{\rm ad}$) are opposite in sign to the angular momentum itself, and therefore decelerate the rotational motions of the magma column. The torque generated by the gas pressure force ($\vec{\mathcal{T}}^{g}$) may have the same sign as $\vec{L}$ (see Fig. 2a), in which case it accelerates the rotational motions. The evolution of the angular momentum is determined by the sum of all three torques

$$\frac{\partial \vec{L}}{\partial t} = \vec{\mathcal{T}}^{\rm vb} + \vec{\mathcal{T}}^{\rm ad} + \vec{\mathcal{T}}^{g} = \vec{\mathcal{T}}^{\rm tot} \tag{12}$$

where the total torque $\vec{\mathcal{T}}^{\rm tot} = \vec{\mathcal{T}}^{\rm vb} + \vec{\mathcal{T}}^{\rm ad} + \vec{\mathcal{T}}^{g}$ can be further calculated using eqs (10) and (11), which becomes

$$\vec{\mathcal{T}}^{\rm tot} = 2\sigma\vec{L} \tag{13}$$

When the system is dominated by any of the three stable perturbations (with $\sigma < 0$), the net torque $\vec{\mathcal{T}}^{\rm tot}$ points in the opposite direction of $\vec{L}$, which damps the rotational motions of the magma column. When the system is dominated by the Bernoulli perturbations (with $\sigma > 0$), the angular momentum increases with time, because the positive and large torque $\vec{\mathcal{T}}^{g}$ causes a propelling net torque $\vec{\mathcal{T}}^{\rm tot}$. In this case, we refer to $\vec{\mathcal{T}}^{g}$ as the 'Bernoulli torque' due to its close link to the Bernoulli effect. Due to the Bernoulli effect, the strength of the Bernoulli torque increases with increasing gas velocity, which is indicated by the higher Mach number (see Fig. 2b).

When the system is dominated by the perturbations with a single growth rate $s = \sigma - i\omega$ and wavenumber k (e.g. after the system has evolved long enough for the decaying perturbations to vanish), the displacement components $u_{x,y}(z, t)$ can be obtained from the waveform solutions $\widehat{u_{x,y}}e^{ikz+st}$, where the complex Fourier coefficients $\widehat{u_x}$ and $\widehat{u_y}$ are determined by the initial displacement of the magma column. In this case, the angular momentum for the perturbations can be expressed as a function of time t and height z (see Appendix B5.2)

$$\vec{L} = \left(\omega|\widehat{u_x}| \cdot |\widehat{u_y}|e^{2\sigma t}\sin\omega(\tau_y^u - \tau_x^u)\right)\hat{z} \tag{14}$$

where $|\widehat{u_x}|$ and $|\widehat{u_y}|$ are the magnitudes of $\widehat{u_x}$ and $\widehat{u_y}$, respectively; and $\tau_{x,y}^u$ are time lags indicating the initial phases of the oscillations along $\hat{x}$ and $\hat{y}$. If the magma column has wagging motions with the perturbations confined to a 2-D vertical plane, then the displacement components u_x and u_y are always proportional to each other and $\tau_x^u - \tau_y^u = n\pi$ ($n = 0, 1, 2, \ldots$). In this case, the angular momentum is always zero. If the gas annulus is impermeable, the Bernoulli torque $\vec{\mathcal{T}}^{g}$ always vanishes (see Appendix B5.2), and the angular momentum decays due to the viscous torques. If the magma column whirls in the conduit with 3-D Bernoulli perturbations, and the annulus is permeable, the rotational motions will be propelled due to the Bernoulli torque. By enabling the Bernoulli effect, the permeable annulus enhances the growth in angular momentum of the whirling magma column.

3.2.2 Evolution of energy under the linear forces

When the system is dominated by a single growth rate $s = \sigma - i\omega$ and wavenumber k, the linear evolution eq. (9c) can be expressed in terms of the real and imaginary parts of s (see Appendix B5.3)

$$\frac{\partial^2 \vec{u}}{\partial t^2} = -(\sigma^2 + \omega^2)\vec{u} + 2\sigma \frac{\partial \vec{u}}{\partial t} \tag{15}$$

which is similar to the evolution equation of a damped harmonic oscillator under a linear drag (if $\sigma < 0$), or propelling (if $\sigma > 0$) force. We define a potential Φ similar to the elastic potential for a harmonic oscillator, a kinetic energy K and the total energy $\mathcal{E}$ as

$$\Phi = \frac{1}{2}u^2(\sigma^2 + \omega^2), \qquad K = \frac{1}{2}\frac{\partial \vec{u}}{\partial t} \cdot \frac{\partial \vec{u}}{\partial t}, \qquad \mathcal{E} \equiv \Phi + K \tag{16}$$

where $u^2 = u_x^2 + u_y^2$. Similar to the torques, we identify the power sources and sinks (i.e. rate of work) corresponding to the linear forces, $\mathcal{W}^{\mathrm{ad,vb},g} = \frac{\partial \vec{u}}{\partial t} \cdot \vec{F}^{\mathrm{ad,vb},g}$, which, for perturbations with a single growth rate s and wavenumber k, become (see Appendix B5.3)

$$\mathcal{W}^{\mathrm{vb}} = -2k^2\eta K \qquad \mathcal{W}^{\mathrm{ad}} = -2(1-\phi_o)\eta\lambda K \qquad \mathcal{W}^{g} = \frac{2\lambda}{\beta}\frac{\mathrm{Im}(\Theta)}{\omega}K \tag{17}$$

The power sinks $\mathcal{W}^{\mathrm{ad}}$ and $\mathcal{W}^{\mathrm{vb}}$ indicate the work done by the viscous forces, which are always negative and thus tend to damp the energy of the magma column. $\mathcal{W}^{g}$ is referred to as the 'Bernoulli power source' for the Bernoulli perturbations, which indicates the positive work done to the magma column by the gas pressure force under the Bernoulli effect. Similar to the Bernoulli torque, the Bernoulli power source increases the total energy of the system under the dominance of the Bernoulli perturbations. The evolution of the energy $\mathcal{E}$ is determined by the sum of all power sources

$$\frac{\partial \mathcal{E}}{\partial t} = \mathcal{W}^{\mathrm{ad}} + \mathcal{W}^{\mathrm{vb}} + \mathcal{W}^{g} = \mathcal{W}^{\mathrm{tot}} \tag{18}$$

where the total power source $\mathcal{W}^{\mathrm{tot}}$ can be further expressed, using eqs (10) and (17), as

$$\mathcal{W}^{\mathrm{tot}} = 4\sigma K \tag{19}$$

Comparing eq. (17) with eq. (11), and eq. (13) with eq. (19), we observe that

$$\frac{\mathcal{W}^{\mathrm{ad,vb},g,\mathrm{tot}}}{2K} = \frac{\vec{\mathcal{T}}^{\mathrm{ad,vb},g,\mathrm{tot}}}{\vec{L}}$$

Therefore, we deduce that, similar to $\mathcal{T}^{g}$, $\mathcal{W}^{g}$ is positive for three out of the four roots of a given wavenumber (as shown in Fig. 2a), and that the Bernoulli power source increases with the gas velocity (Fig. 2b); for the Bernoulli perturbations, $\mathcal{W}^{g}$ is strong enough to yield a positive $\mathcal{W}^{\mathrm{tot}}$, hence causing the energy of the magma column to increase. The evolutions of energy and angular momentum in our linear analysis show that the Bernoulli effect, which causes the Bernoulli perturbations to grow, also promotes the growth in both angular momentum and energy of the magma column. Note that if the system contains multiple wavelengths or frequencies (e.g. just after an unrest when decaying perturbations have not subsided yet), the torques and power sources acting on the magma column consist of quadratic non-linear products between different perturbations. However, due to the growing Bernoulli perturbations, both the energy and angular momentum contain at least one exponentially growing component, and become subjected to the Bernoulli torque and Bernoulli power source, as time proceeds. During the growth of energy and angular momentum, the displacement amplitude of the magma column becomes larger and larger. The large displacement eventually leads to non-linear damping effects that are negligible with small displacement but are prominent with large displacement. These effects will be discussed in the following section.

4 NON-LINEAR ANNULAR DAMPING

When the magnitude u of the magma column's displacement increases due to the Bernoulli effect and the approximation $u^2 \ll 1$ no longer satisfies, the non-linear effects caused by large u become important. As the displacement grows, the most compressed section along the annulus has thickness $1 - u$. The non-linear annulus drag force $F^{\mathrm{ad}} \propto \frac{1}{1-u}$ increases rapidly with u, causing stronger resistance when the annulus is pinched towards the conduit wall. Because the viscous bending force and gas force $\vec{F}^{\mathrm{vb},g}$ change less rapidly with larger u (remain finite, while $\vec{F}^{\mathrm{ad}}$ becomes infinite at $u \to 1$), the increase of $\vec{F}^{\mathrm{ad}}$ can lead to a stronger damping torque and power sink, which may cause the angular momentum $\vec{L}$ and energy $\mathcal{E}$ of the magma column to decrease when u is large enough.

4.1 The effect of non-linear damping on angular momentum and energy

At large displacement of the magma column, the annulus drag force $\vec{F}^{\mathrm{ad}}$ contributes to a non-linear torque and power source according to

$$\vec{\mathcal{T}}^{\mathrm{ad}} = \vec{u} \times \vec{F}^{\mathrm{ad}}, \qquad \mathcal{W}^{\mathrm{ad}} = \frac{\partial \vec{u}}{\partial t} \cdot \vec{F}^{\mathrm{ad}} \tag{20}$$

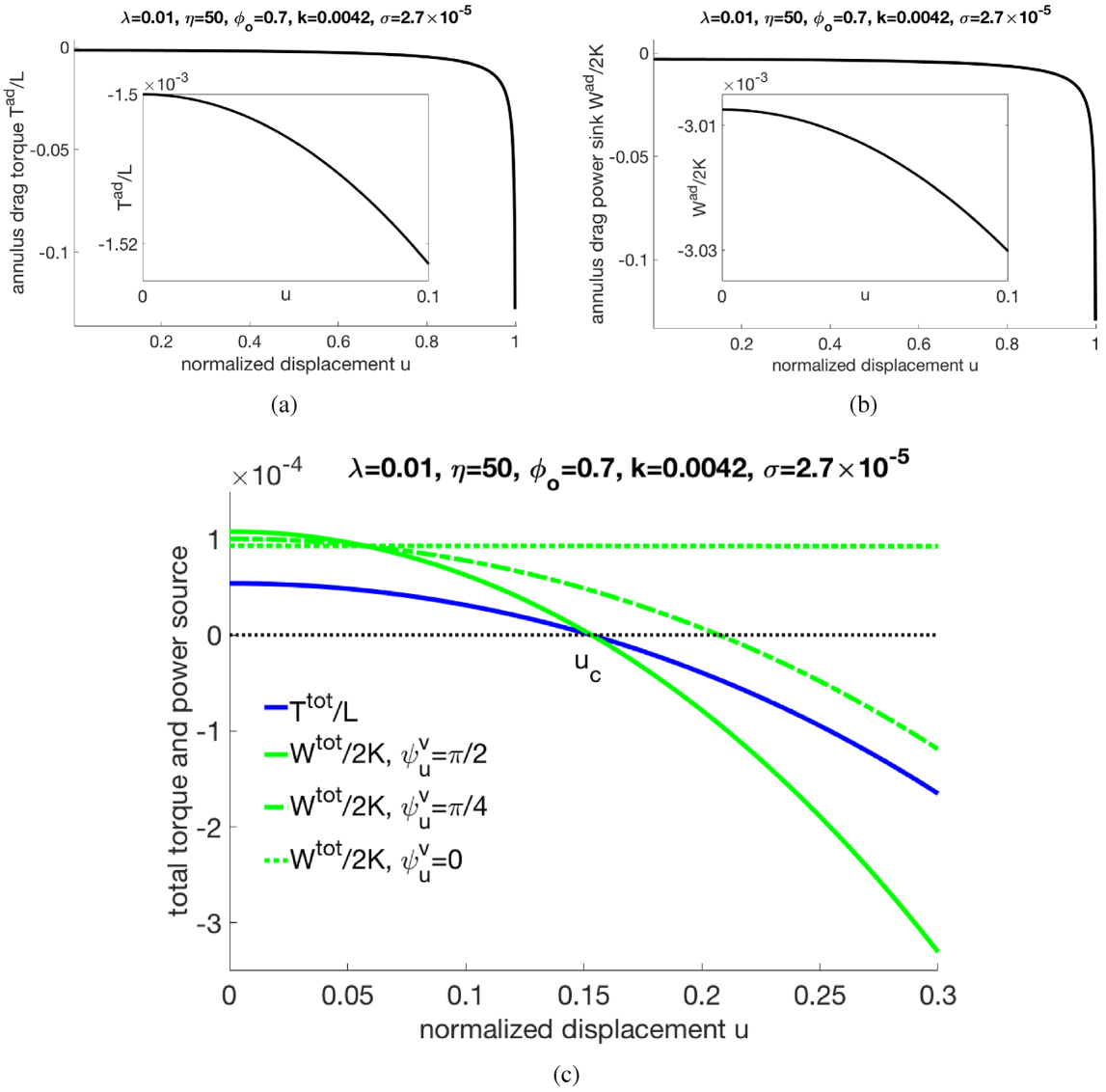

Figure 3. Torques and rates of work done to the magma column dominated Bernoulli perturbations with wavenumber $k = 0.0042$. Frame (a) shows the annulus drag torque $\vec{\mathcal{T}}^{\rm ad}/\vec{L}$, and frame (b) shows the annulus drag power sink $\mathcal{W}^{\rm ad}/2K$ as functions of the dimensionless displacement amplitude u. Insets in (a) and (b) are zoom-in of the curves over small values of u. A near-circular trajectory (i.e. angle $\psi_u^v = \pi/2$) is assumed when calculating the torque and power sink. Frame (c) shows the total torque $\vec{\mathcal{T}}^{\rm tot}/\vec{L}$ (blue curve), and total power source $\mathcal{W}^{\rm tot}/2K$ (green curves) as functions of u. The total power source/sink is calculated for three different whirling trajectories represented by the value of angle ψ_u^v between the displacement $\vec{u}$ and the velocity $\vec{v}$ of the magma column: a 2-D trajectory ($\psi_u^v = 0$), a near circular trajectory ($\psi_u^v = \pi/2$) and an elliptical trajectory ($\psi_u^v = \pi/4$). The total torque and power source (for circular trajectory) cross zero (black dash line) at the critical displacement u_c. The values of non-linear torques and power sources are calculated according to eqs (C5) and (C9) in Appendix C1.

Similar to their linear forms, the non-linear torque $\vec{\mathcal{T}}^{\rm ad}$ and power source $\mathcal{W}^{\rm ad}$ have opposite signs to that of $\vec{L}$ and $\mathcal{E}$. Meanwhile, their magnitudes $|\vec{\mathcal{T}}^{\rm ad}|$ and $|\mathcal{W}^{\rm ad}|$ monotonically increase with u (Figs 3 a and b). As a result, the non-linear damping of the motions of the magma column becomes more rapid as u increases.

Because $\vec{\mathcal{T}}^{\rm ad}$ and $\mathcal{W}^{\rm ad}$ change far more drastically (which could approach infinity when $u \to 1$) than $\vec{\mathcal{T}}^{\rm vb,g}$ and $\mathcal{W}^{\rm vb,g}$ (which remain finite), we approximate the later torques and power sources using their linear forms. With these approximations, we calculate the changes in the total torque $\vec{\mathcal{T}}^{\rm tot}$ and power source $\mathcal{W}^{\rm tot}$ at large displacement by substituting the linear forms of $\vec{\mathcal{T}}^{\rm ad}$ and $\mathcal{W}^{\rm ad}$ by their non-linear counterparts (see Appendix C1 for details).

When the displacement magnitude u increases, $\vec{\mathcal{T}}^{\rm tot}$ transitions from being propelling (positive) to damping (negative) when the magnitude of the magma column reaches a critical value u_c such that $\vec{\mathcal{T}}^{\rm tot}(u_c) = 0$ (see Fig. 3 c and Fig. C1 in Appendix C1 for more parameters). Once when $u > u_c$, the damping of the angular momentum begins. Similarly, for the damping of the energy of the magma column, we can define a critical displacement magnitude, beyond which the power source becomes a power sink. Specifically, if the trajectory of the magma column is near circular (i.e. the displacement $\vec{u}$ is perpendicular to the velocity $\vec{v} = \frac{\partial \vec{u}}{\partial t}$ and the angle between them $\psi_u^v = \pi/2$ or $3\pi/2$), the total power source and the total torque transition at the same critical displacement u_c. If the trajectory of the magma column section is elliptical,

the transition in $\mathcal{W}^{\text{tot}}$ is delayed and occurs at a magnitude larger than u_c. An exception occurs when the trajectory of the magma column is 2-D and free of angular momentum (i.e. $\vec{u}$ and $\vec{v}$ are parallel with $\psi_u^v = 0$ or π): in this case, $\mathcal{W}^{\text{tot}}$ may remain positive even when the displacement of the magma column reaches the maximum value permitted by the system ($u = 1$), resulting in the column colliding with the conduit wall and its motion halted upon collision (Fig. 3c).

4.2 Re-excitation of high-frequency modes and timescales of non-linear damping

Using the critical displacement u_c for the total torque and total power source (for near-circular trajectory), we define a critical growth time t_c to be the time it takes for the displacement magnitude u to increase from its initial value to the critical displacement u_c. If the Bernoulli perturbations correspond to an initial displacement magnitude u_o at $t = 0$, the critical growth time t_c can be approximated by

$$u_o e^{\sigma t_c} = u_c \tag{21}$$

where σ is the growth rate of the Bernoulli perturbation. The non-linear effect can lead to re-excitations of linear perturbations: when $t > t_c$, the rapid damping of energy and angular momentum is likely to soon decrease u back to a small value and restore the magma column to the linear regime. As the magma column re-enters the linear regime, the instantaneous values ($\vec{u}$, $\vec{v}$, ρ, w), now resulting from the non-linear damping, form a new set of initial perturbations and redistribute among perturbations with different frequencies, starting a new round of oscillations. We can identify the cycle of the whirling motions to be from the onset of initial perturbations to the restoration of small displacements of the magma column, and t_c can be viewed as a midpoint through this process. The non-linear damping towards the end of each whirling cycle can be viewed as a process of generating the initial conditions of the next cycle. As a result, the Bernoulli effect and the non-linear damping effect together contribute to a self-sustained wagging mechanism.

The length of the whirling cycle is determined by the physical properties of the conduit, as well as the velocity W_o of the unperturbed gas flux. When gas exsolution intensifies in the volcanic conduit, the velocity of the gas flux becomes larger, resulting in larger u_c (Fig. 4a). The magma column therefore can reach further towards to the conduit wall, which potentially leads to larger amplitudes in seismic pressure waves (Liao *et al.* 2018), before the non-linear damping becomes important. However, as the growth rate σ increases with the gas flux velocity significantly, the magma column can reach u_c more rapidly, hence the growth time t_c decreases (Fig. 4b). As discussed in previous studies, as the volcano becomes more active, the annulus thins, since the magma becomes shear weakening with greater vesiculation (Jellinek & Bercovici 2011; Gonnermann & Manga 2007). For a volcanic conduit with fixed outer radius R_c and gas injection velocity, the thinning of the annulus causes a decrease in u_c (Fig. 4c) as well as t_c (Fig. 4d). When the annulus thickness is fixed, the critical displacement and growth time both increase for bigger conduit radii (Figs 4 c and d).

When the unrest of the volcano intensifies en route to an eruption, the gas flux velocity increases, and the vesicular annulus becomes thinner. Therefore, the length of each whirling cycle (approximated by $2t_c$), becomes shorter. Meanwhile, during each whirling cycle, the seismic signals associated with the motions of the magma column first intensify due to the Bernoulli perturbations (when $t < t_c$), and then decrease due to the non-linear damping (when $t > t_c$). This non-monotonic evolution in time is similar to that for the chugging events observed in seismic tremor. Considering a system with magma density $\rho_m \sim 2.85 \times 10^3 \text{kgm}^-3$, magma viscosity $\mu_m \sim 10^7 \text{Pas}$, isothermal sound speed $C_g \sim 700\,\text{ms}^{-1}$, magma to gas density ratio $\rho_m/\rho_o \sim 100$, the length of a whirling cycle $2t_c$ can range from seconds to over a minute for varying conduit radius and annulus width (see Figs 4 b and d). This time range overlaps those observed for chugging envelopes in seismic tremor from seconds to tens of seconds (Johnson & Lees 2000).

5 SUMMARY AND DISCUSSION

Following the existing 3-D extension of the gas-flux-free whirling model (Liao *et al.* 2018), and the 2-D wagging model with gas flux (Bercovici *et al.* 2013), we examine the motion of magma column in three dimensions in the presence of gas flux through a permeable vesicular annulus. Similar to the findings of Bercovici *et al.* (2013), we find that gas flux through the annulus induces instabilities in the displacement of the magma column, as well as the density and velocity of the gas in the annulus. We refer to these instabilities as the Bernoulli perturbations, which originate from the Bernoulli effect in the gas flux flowing through the permeable and deformable annulus. We further find that when the Bernoulli perturbations dominate the system, the gas pressure causes a positive torque (Bernoulli torque), and provides positive work (Bernoulli power source) acting on the magma column, hence increasing both its angular momentum and energy.

As the system evolves, the dominance of the Bernoulli perturbations causes the amplitudes of waves in the magma column's displacement to grow exponentially. When the displacement of the magma column becomes large enough and reaches a critical value u_c, a non-linear drag force from shear across the annulus becomes important, resulting in rapid damping of the energy and angular momentum of the magma column. An exception occurs when the magma column undergoes 2-D, side-to-side wagging motion, in which case the non-linear damping does not effectively reduce the energy of the column. As a result, the wagging column could eventually collide with the conduit wall before its displacement decreases. The pinching of the annulus and the contact between the magma column and the conduit wall, in this case, may lead to partial destruction of the annulus structure, which may further disturb the wagging motion. When the magma column whirls in three dimensions, the non-linear damping sends the magma column back to its linear regime where its displacement is small, and a new cycle of perturbations starts again.

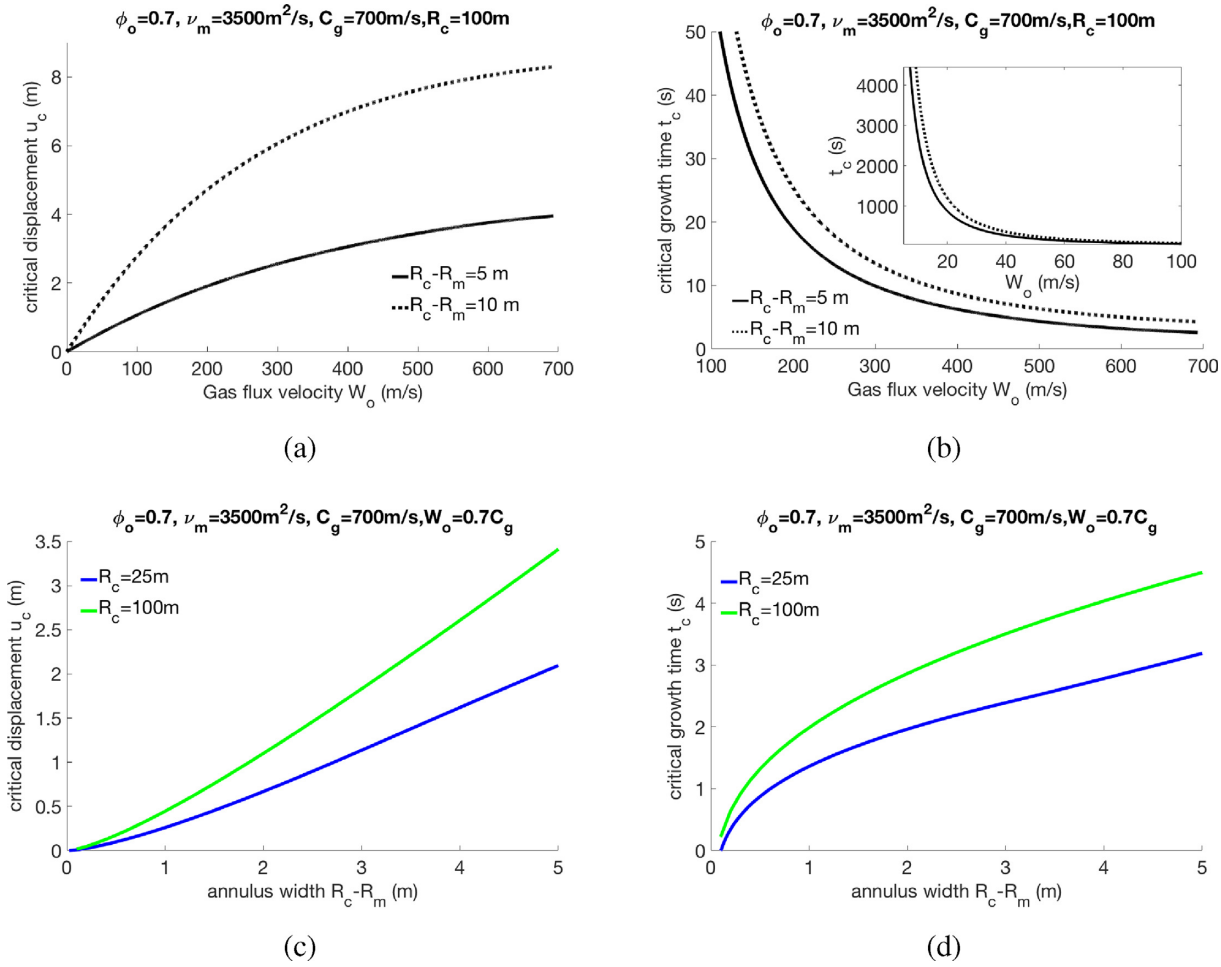

Figure 4. Critical displacement u_c (in metres) and corresponding critical growth time t_c (in seconds), for a system with initial column displacement $u_o \sim 1$ cm. Frame (a) shows the critical displacement u_c as a function of gas injection velocity W_o in two cases with different annulus widths. Frame (b) shows the critical growth time t_c as a function of W_o for two different annulus widths. The inset in (b) shows the same curve over smaller values of W_o. Frames (c) and (d) show the critical displacement u_c and the growth time t_c as functions of the annulus width $R_c - R_m$, respectively, for two different conduit radii $R_c = 25$ and 100 m. For each case, the Bernoulli perturbations with the maximum growth rate among all wavenumbers is selected to calculate u_c and t_c.

The Bernoulli effect and the annulus damping effect contribute to different regimes of a self-sustained excitation mechanism: due to the Bernoulli effect, the motion of the magma column can intensify, causing detectable pressure waves that transmit away from the conduit; due to the non-linear damping effect, the motion of the magma column is self-regulated, so that oscillations with similar frequencies to those of seismic tremor can be periodically regenerated (see Appendix B2). We also note that the presence of the non-linear damping can maintain the integrity of the gas annulus, by preventing the whirling of the magma column to grow until the annulus is destroyed. The evolution of whirling predicted by the excitation mechanism, which involves cycles of first increasing and then decreasing intensity of whirling, is similar in frequency to the 'chugging'events observed in seismic tremor, which are characterized by envelopes of high-amplitude seismic signals (Johnson & Lees 2000). The typical length of a chugging envelope, which range from seconds to tens of seconds, is consistent with the prediction on the length of the whirling cycles using our model.

ACKNOWLEDGEMENTS

This work was supported by National Science Foundation grants EAR-1344538 and EAR-1645057

REFERENCES

Bercovici, D. & Michaut, C., 2010. Two-phase dynamics of volcanic eruptions: compaction, compression, and the conditions for choking, *Geophys. J. Int.,* **182,** 843–864.

Bercovici, D., Jellinek, A.M., Michaut, C., Roman, D.C. & Morse, R., 2013. Volcanic tremors and magma wagging: gas flux interactions and forcing mechanism, *Geophys. J. Int.,* **195**(2), 1001–1022.

Garcés, M., Hagerty, M. & Schwartz, S., 1998. Magma acoustics and time-varying melt properties at Arenal Volcano, Costa Rica, *Geophys. Res. Lett.,* **25**(13), 2293–2296.

Gonnermann, H.M. & Manga, M., 2007. The fluid mechanics inside a volcano, *Annu. Rev. Fluid Mech.,* **39,** 321–356.

Jellinek, A.M. & Bercovici, D., 2011. Seismic tremors and magma wagging during explosive volcanism, *Nature,* **470**(7335), 522–525.

Johnson, J. & Lees, J., 2000. Plugs and chugs—seismic and acoustic observations of degassing explosions at Karymsky, Russia and Sangay, Ecuador, *J. Volc. Geotherm. Res.,* **101**(1), 67–82.

Konstantinou, K. & Schlindwein, V., 2003. Nature, wavefield properties and source mechanism of volcanic tremor: a review, *J. Volc. Geotherm. Res.,* **119**(1–4), 161–187.

Lesage, P., Mora, M.M., Alvarado, G.E., Pacheco, J. & Métaxian, J.-P., 2006. Complex behavior and source model of the tremor at arenal volcano, costa rica, *J. Volc. Geotherm. Res.,* **157**(1), 49–59.

Liao, Y., Bercovici, D. & Jellinek, M., 2018. Magma wagging and whirling in volcanic conduits, *J. Volc. Geotherm. Res.,* **351,** 51–74.

McNutt, S., 2005. Volcanic seismology, *Annu. Rev. Earth Planet. Sci.,* **32,** 461–491.

Nadeau, P.A., Palma, J.L. & Waite, G.P., 2011. Linking volcanic tremor, degassing, and eruption dynamics via SO_2 imaging, *Geophys. Res. Lett,* **38,** doi:10.1029/2010GL045820.

Zuccarello, L., Burton, M.R., Saccorotti, G., Bean, C.J. & Patanè, D., 2013. The coupling between very long period seismic events, volcanic tremor, and degassing rates at mount etna volcano, *J. geophys. Res.,* **118**(9), 4910–4921.

APPENDIX A: THEORETICAL FRAMEWORK

A1 Model set-up

Following previous magma wagging models (Jellinek & Bercovici 2011; Liao *et al.* 2018), we assume that inside the volcanic conduit with radius R_c, a magma column with radius R_m is enveloped by a gas-rich foamy annulus with width $R_c - R_m$. The displacement of the magma column in three dimensions is represented by its displacement vector $\vec{u}(z, t)$ at time t and height z along the column (Fig. 1). In cylindrical-polar coordinates, $\vec{u}$ is expressed using its magnitude u and its polar angle ψ_u (Fig. A1a).

For an arbitrary point Q on the surface of the magma column with polar angle of θ (Fig. A1a), its position $\vec{r}_m$ (Fig. A1b) satisfies $R_m = |\vec{r}_m - \vec{u}|$, leading to

$$r_m(\theta) = u\cos\Delta\theta + \sqrt{R_m^2 - u^2\sin^2\Delta\theta} \tag{A1}$$

where $\Delta\theta = \theta - \psi_u$ represents the angle between the displacement vector $\vec{u}$ and $\vec{r}_m$. The expression for r_m in eq. (A1) straightforwardly leads to the expressions for r_m^2 and r_m^3

$$\begin{aligned} r_m^2 &= R_m^2 - u^2 + 2u\cos\Delta\theta\left(u\cos\Delta\theta + \sqrt{R_m^2 - u^2\sin^2\Delta\theta}\right) \\ r_m^3 &= 3u(R_m^2 - u^2)\cos\Delta\theta + 4u^3\cos^3\Delta\theta + (R_m^2 + 3u^2 - 4u^2\sin^2\Delta\theta)\sqrt{R_m^2 - u^2\sin^2\Delta\theta} \end{aligned} \tag{A2}$$

We identify the unit vector $\hat{n}$, which is perpendicular to the surface element at Q, and the unit vector $\hat{t}$, which is parallel to the surface element. The two unit vectors are (see Fig. 1b)

$$\begin{aligned} \hat{n}(\theta) &= (\vec{r}_m - \vec{u})/R_m \\ \hat{t}(\theta) &= \hat{z}\times\hat{n} \end{aligned} \tag{A3}$$

where $\hat{z} = (0, 0, 1)$ is the unit vector along the vertical direction. The local unit vectors $\hat{n}$ and $\hat{t}$ defined in eq. (A3) have geometrical relations with the direction of the magma column's displacement:

$$\begin{aligned} \hat{u}\cdot\hat{n} &= \hat{z}\cdot\left(\hat{u}\times\hat{t}\right) = \frac{r_m}{R_m}\cos\Delta\theta - \frac{u}{R_m} \\ \hat{u}\cdot\hat{t} &= -\hat{z}\cdot(\hat{u}\times\hat{n}) = -\frac{r_m}{R_m}\sin\Delta\theta \end{aligned} \tag{A4}$$

where $\hat{u} = \vec{u}/u$ is the unit vector along the direction of the displacement $\vec{u}$.

In the following text, we will use the vector operations and definitions

$$\angle_{\hat{a}}^{\hat{b}} = \angle_{\hat{a}}^{\hat{c}} + \angle_{\hat{c}}^{\hat{b}} = \angle_{\hat{a}}^{\hat{c}} - \angle_{\hat{b}}^{\hat{c}} \tag{A5a}$$

$$\cos\angle_{\hat{a}}^{\hat{b}} = \hat{a}\cdot\hat{b} = \frac{\vec{a}\cdot\vec{b}}{ab}, \qquad \sin\angle_{\hat{a}}^{\hat{b}} = \hat{z}\cdot\left(\hat{a}\times\hat{b}\right) = \frac{\hat{z}\cdot(\vec{a}\times\vec{b})}{ab} \tag{A5b}$$

where $\vec{a}$ and $\vec{b}$ are arbitrary vectors on the horizontal plane, whose amplitudes are a and b, respectively. $\hat{a} = \vec{a}/a$ and $\hat{b} = \vec{b}/b$ are the unit vectors along the directions of $\vec{a}$ and $\vec{b}$, and $\hat{c}$ is an unit vector along an arbitrary direction. We define $\angle_{\hat{a}}^{\hat{b}}$ as the polar angle obtained by rotating $\hat{a}$, in the counterclockwise direction, till it aligns with $\hat{b}$.

A2 Forces on the magma column

For any section of the magma column with thickness dz, the column section is subjected to a gas pressure force $\vec{F}^g$, which arises from non-uniform gas density variation in the deformed vesicular annulus. For a small surface element on the magma column at point Q (Fig. A1a), the pressure force acting on the surface element points towards the centre of the magma column. The pressure force has a magnitude $P(\theta)$dS,

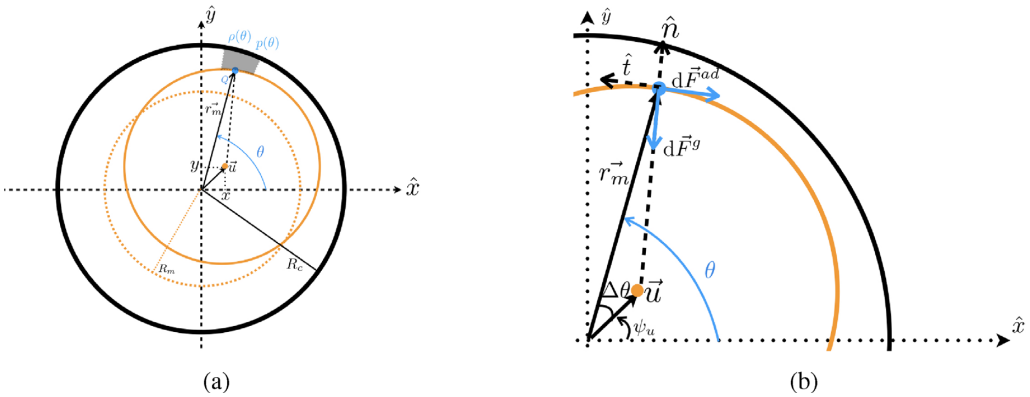

Figure A1. Frame (a) shows the intersection of the conduit (black line) and the magma column (orange line). Q is an arbitrary point on the surface of the magma column. Grey shaded area indicates a section of the annulus with angular position θ. The undisturbed position of the magma column is indicated by the orange dash line. Frame (b) shows the pressure force and annulus drag force, generated in the annulus section, acting on the interface between the annulus section and magma column.

where $P(\theta)$ is the gas pressure in the deformed annulus section measured at θ, and dS is the area of the surface element spanned by dθ. The motion of the column also generates a shear stress at Q, which can be approximated as $\mu(\theta)\frac{\vec{v}\cdot\hat{t}}{R_c-R_m}$, where $\vec{v}=\frac{\partial\vec{u}}{\partial t}$ is the velocity of the magma column section, and $\mu(\theta)$ is the viscosity of the annulus, primarily controlled by the magma matrix. Assuming the gas annulus is at constant temperature due to the high heat capacity of the magma, then the gas pressure force $\mathrm{d}\vec{F}^g$ and drag force $\mathrm{d}\vec{F}^{\mathrm{ad}}$ acting on the same column surface can be further expressed as

$$\begin{aligned}\mathrm{d}\vec{F}^g &= -C_g^2\rho(\theta)r_m\mathrm{d}\theta\mathrm{d}z\hat{n}\\ \mathrm{d}\vec{F}^{\mathrm{ad}} &= -\mu(\theta)r_m\mathrm{d}\theta\mathrm{d}z\frac{\vec{v}\cdot\hat{t}}{R_c-r_m}\hat{t}\end{aligned}\tag{A6}$$

where C_g is the isothermal sound speed of the gas in the annulus, and the term $r_m\mathrm{d}\theta\mathrm{d}z$ represents the area of the surface element dS spanned by angular increment dθ and vertical increment dz.

The pressure and viscous drag forces can be further expressed as $\mathrm{d}\vec{F}^g=\mathrm{d}F_u^g\hat{u}+\mathrm{d}F_\psi^g\hat{\psi}$ and $\mathrm{d}\vec{F}^{\mathrm{ad}}=\mathrm{d}F_u^{\mathrm{ad}}\hat{u}+\mathrm{d}F_\psi^{\mathrm{ad}}\hat{\psi}$, where $\hat{u}$ and $\hat{\psi}=\hat{z}\times\hat{u}$ are the perpendicular bases in polar coordinates. The radial and tangential components for both forces can be calculated according to $\mathrm{d}F_u^{g,\mathrm{ad}}=\hat{u}\cdot\mathrm{d}\vec{F}^{g,\mathrm{ad}}$ and $\mathrm{d}F_\psi^{g,\mathrm{ad}}=\hat{z}\cdot\left(\hat{u}\times\mathrm{d}\vec{F}^{g,\mathrm{ad}}\right)$, which lead to

$$\mathrm{d}F_u^g=-(\hat{u}\cdot\hat{n})C_g^2\rho(\theta)r_m\mathrm{d}\theta\mathrm{d}z,\qquad \mathrm{d}F_\psi^g=-\hat{z}\cdot(\hat{u}\times\hat{n})\,C_g^2\rho(\theta)r_m\mathrm{d}\theta\mathrm{d}z\tag{A7a}$$

$$\mathrm{d}F_u^{\mathrm{ad}}=-(\hat{u}\cdot\hat{t})\mu(\theta)r_m\mathrm{d}\theta\mathrm{d}z\frac{\vec{v}\cdot\hat{t}}{R_c-r_m},\qquad \mathrm{d}F_\psi^{\mathrm{ad}}=-\hat{z}\cdot\left(\hat{u}\times\hat{t}\right)\mu(\theta)r_m\mathrm{d}z\mathrm{d}\theta\frac{\vec{v}\cdot\hat{t}}{R_c-r_m}\tag{A7b}$$

Substitute eqs (A1) and (A4) into eq. (A7a), we expand the pressure force components in eq. (A7a) as

$$\begin{aligned}\mathrm{d}F_u^g &= -C_g^2\rho(\theta)\mathrm{d}\theta\mathrm{d}z\left(u\cos\Delta\theta+\sqrt{R_m^2-u^2\sin^2\Delta\theta}\right)\left(\frac{u\cos\Delta\theta+\sqrt{R_m^2-u^2\sin^2\Delta\theta}}{R_m}\cos\Delta\theta-\frac{u}{R_m}\right)\\ &= \frac{C_g^2\rho(\theta)(u^2-R_m^2)}{R_m}\cos\Delta\theta\mathrm{d}\theta\mathrm{d}z-\frac{C_g^2\rho(\theta)u}{R_m}\cos2\Delta\theta\left(u\cos\Delta\theta+\sqrt{R_m^2-u^2\sin^2\Delta\theta}\right)\mathrm{d}\theta\mathrm{d}z\\ \mathrm{d}F_\psi^g &= -C_g^2\rho(\theta)\mathrm{d}\theta\mathrm{d}z\left(u\cos\Delta\theta+\sqrt{R_m^2-u^2\sin^2\Delta\theta}\right)\frac{u\cos\Delta\theta+\sqrt{R_m^2-u^2\sin^2\Delta\theta}}{R_m}\sin\Delta\theta\\ &= \frac{-C_g^2\rho(\theta)\mathrm{d}\theta\mathrm{d}z}{R_m}\left(2u^2\cos^2\Delta\theta\sin\Delta\theta+(R_m^2-u^2)\sin\Delta\theta+2u\sin\Delta\theta\cos\Delta\theta\sqrt{R_m^2-u^2\sin^2\Delta\theta}\right)\\ &= \frac{C_g^2\rho(\theta)(u^2-R_m^2)}{R_m}\sin\Delta\theta\mathrm{d}\theta\mathrm{d}z-\frac{C_g^2\rho(\theta)u}{R_m}\sin2\Delta\theta\left(u\cos\Delta\theta+\sqrt{R_m^2-u^2\sin^2\Delta\theta}\right)\mathrm{d}\theta\mathrm{d}z\end{aligned}\tag{A8}$$

Using the relation (A5a), we expand the components of the viscous drag force eq. (A7b) as

$$\begin{aligned}
\mathrm{d}F_u^{\mathrm{ad}} &= -(\hat{u}\cdot\hat{t})\mu(\theta)r_m\mathrm{d}\theta\mathrm{d}z\frac{v\cos\left(\angle_{\hat{v}}^{\hat{u}}+\angle_{\hat{u}}^{\hat{t}}\right)}{R_c-r_m}\\
&= -(\hat{u}\cdot\hat{t})\mu(\theta)r_m\mathrm{d}\theta\mathrm{d}z v\frac{(\hat{v}\cdot\hat{u})(\hat{u}\cdot\hat{t})+(\hat{u}\times\hat{v})\cdot(\hat{u}\times\hat{t})}{R_c-r_m}\\
\mathrm{d}F_\psi^{\mathrm{ad}} &= -\hat{z}\cdot\left(\hat{u}\times\hat{t}\right)\mu(\theta)r_m\mathrm{d}\theta\mathrm{d}z\frac{v\cos\left(\angle_{\hat{v}}^{\hat{u}}+\angle_{\hat{u}}^{\hat{t}}\right)}{R_c-r_m}\\
&= -\hat{z}\cdot\left(\hat{u}\times\hat{t}\right)\mu(\theta)r_m\mathrm{d}\theta\mathrm{d}z v\frac{(\hat{v}\cdot\hat{u})(\hat{u}\cdot\hat{t})+(\hat{u}\times\hat{v})\cdot(\hat{u}\times\hat{t})}{R_c-r_m}
\end{aligned}\tag{A9}$$

Substituting eqs (A4) and (A2) into eq. (A9), the components of the viscous drag force are further expanded as

$$\begin{aligned}
\mathrm{d}F_u^{\mathrm{ad}} &= -\frac{(\hat{u}.\hat{v})}{R_m^2}\frac{\mu(\theta)\mathrm{d}\theta\mathrm{d}z}{R_c-r_m}v\left(3u(R_m^2-u^2)\sin^2\Delta\theta\cos\Delta\theta+4u^3\sin^2\Delta\theta\cos^3\Delta\theta\right)\\
&\quad+\frac{\hat{z}\cdot(\hat{u}\times\hat{v})}{R_m^2}\frac{\mu(\theta)\mathrm{d}\theta\mathrm{d}z}{R_c-r_m}v\left(u(3R_m^2-5u^2)\cos^2\Delta\theta\sin\Delta\theta-u(R_m^2-u^2)\sin\Delta\theta+4u^3\cos^4\Delta\theta\sin\Delta\theta\right)\\
&\quad-\frac{(\hat{u}.\hat{v})}{R_m^2}\frac{\mu(\theta)\mathrm{d}\theta\mathrm{d}z}{R_c-r_m}v\left((R_m^2+3u^2)\sin^2\Delta\theta-4u^2\sin^4\Delta\theta\right)\sqrt{R_m^2-u^2\sin^2\Delta\theta}\\
&\quad+\frac{\hat{z}\cdot(\hat{u}\times\hat{v})}{R_m^2}\frac{\mu(\theta)\mathrm{d}\theta\mathrm{d}z}{R_c-r_m}v\left((R_m^2+u^2)\sin\Delta\theta\cos\Delta\theta-4u^2\sin^3\Delta\theta\cos\Delta\theta\right)\sqrt{R_m^2-u^2\sin^2\Delta\theta}\\
\mathrm{d}F_\psi^{\mathrm{ad}} &= -\frac{(\hat{u}.\hat{v})}{R_m^2}\frac{\mu(\theta)\mathrm{d}\theta\mathrm{d}z}{R_c-r_m}v\left(u(R_m^2-u^2)\sin\Delta\theta+u(5u^2-3R_m^2)\sin\Delta\theta\cos^2\Delta\theta-4u^3\sin\Delta\theta\cos^4\Delta\theta\right)\\
&\quad-\frac{\hat{z}\cdot(\hat{u}\times\hat{v})}{R_m^2}\frac{\mu(\theta)\mathrm{d}\theta\mathrm{d}z}{R_c-r_m}v\left(u(3R_m^2-7u^2)\cos^3\Delta\theta+u(3u^2-2R_m^2)\cos\Delta\theta+4u^3\cos^5\Delta\theta\right)\\
&\quad+\frac{(\hat{u}.\hat{v})}{R_m^2}\frac{\mu(\theta)\mathrm{d}\theta\mathrm{d}z}{R_c-r_m}v\left((u^2+R_m^2)\sin\Delta\theta\cos\Delta\theta-4u^2\sin^3\Delta\theta\cos\Delta\theta\right)\sqrt{R_m^2-u^2\sin^2\Delta\theta}\\
&\quad-\frac{\hat{z}\cdot(\hat{u}\times\hat{v})}{R_m^2}\frac{\mu(\theta)\mathrm{d}\theta\mathrm{d}z}{R_c-r_m}v\left((R_m^2-u^2)\cos^2\Delta\theta-4u^2\sin^2\Delta\theta\cos^2\Delta\theta+u^2\right)\sqrt{R_m^2-u^2\sin^2\Delta\theta}
\end{aligned}\tag{A10}$$

in which the column's displacement magnitude u allowed in the conduit has a maximum value of $R_c - R_m$ (i.e. the width of the vesicular annulus). When the annulus is thin compared to the magma column such that $(R_c - R_m)/R_m << 1$, we assume a moderate displacement magnitude $O(\frac{u^2}{R_m^2}) \sim 0$. Under this assumption, we substitute eq. (A1) for r_m, and reduce the expressions for the pressure force components (A8) and the annulus drag force components (A10) to

$$\mathrm{d}F_u^g = -C_g^2R_m\rho(\theta)\cos\Delta\theta\mathrm{d}\theta\mathrm{d}z - C_g^2u\rho(\theta)\cos2\Delta\theta\mathrm{d}\theta\mathrm{d}z \tag{A11a}$$

$$\mathrm{d}F_\psi^g = -C_g^2R_m\rho(\theta)\sin\Delta\theta\mathrm{d}\theta\mathrm{d}z - C_g^2u\rho(\theta)\sin2\Delta\theta\mathrm{d}\theta\mathrm{d}z \tag{A11b}$$

$$\begin{aligned}
\mathrm{d}F_u^{\mathrm{ad}} &= -\tfrac{(\hat{u}\cdot\hat{v})\mu(\theta)\mathrm{d}\theta\mathrm{d}z}{R_m^2(R_c-R_m-u\cos\Delta\theta)}v\left(R_m^3+3uR_m^2\cos\Delta\theta-R_m^3\cos^2\Delta\theta-3uR_m^2\cos^3\Delta\theta\right)\\
&\quad+\tfrac{\hat{z}\cdot(\hat{u}\times\hat{v})\mu(\theta)\mathrm{d}\theta\mathrm{d}z}{R_m^2(R_c-R_m-u\cos\Delta\theta)}v\left(R_m^3\sin\Delta\theta\cos\Delta\theta+3uR_m^2\sin\Delta\theta\cos^2\Delta\theta-uR_m^2\sin\Delta\theta\right)
\end{aligned}\tag{A11c}$$

$$\begin{aligned}
\mathrm{d}F_\psi^{\mathrm{ad}} &= -\frac{\hat{z}\cdot(\hat{u}\times\hat{v})(1-\phi_o)\mu(\theta)\mathrm{d}\theta\mathrm{d}z}{R_m^2(R_c-R_m-u\cos\Delta\theta)}v\left(-2uR_m^2\cos\Delta\theta+R_m^3\cos^2\Delta\theta+3uR_m^2\cos^3\Delta\theta\right)\\
&\quad-\frac{(\hat{u}\cdot\hat{v})(1-\phi_o)\mu(\theta)\mathrm{d}\theta\mathrm{d}z}{R_m^2(R_c-R_m-u\cos\Delta\theta)}v\left(uR_m^2\sin\Delta\theta-3uR_m^2\sin\Delta\theta\cos^2\Delta\theta-R_m^3\sin\Delta\theta\cos\Delta\theta\right)
\end{aligned}\tag{A11d}$$

The total pressure and drag forces can also be expressed in polar coordinate as $\vec{F}^{g,\mathrm{ad}} = F_u^{g,\mathrm{ad}}\hat{u} + F_\psi^{g,\mathrm{ad}}\hat{\psi}$, where the radial and tangential components are obtained by integrations along the annulus

$$F_u^g = \int_{\theta=0}^{2\pi}\mathrm{d}F_u^g, \qquad F_\psi^g = \int_{\theta=0}^{2\pi}\mathrm{d}F_\psi^g \tag{A12a}$$

$$F_u^{\mathrm{ad}} = \int_{\theta=0}^{2\pi}\mathrm{d}F_u^{\mathrm{ad}} \qquad F_\psi^{\mathrm{ad}} = \int_{\theta=0}^{2\pi}\mathrm{d}F_\psi^{\mathrm{ad}} \tag{A12b}$$

Note that as $\rho(\theta)$ is azimuthally periodic along the annulus $\rho(\theta + 2m\pi) = \rho(\theta)$ ($m = 1, 2, 3, \dots$), it can be expressed using discrete Fourier series shown in eq. (A32a)

$$\rho = \rho_o + \sum_{m=1}^{\infty} \left(\rho_m^c \cos m\theta + \rho_m^s \sin m\theta\right) \tag{A13}$$

Substituting eq. (A13) into eqs (A11a) and (A11b), we integrate according to eq. (A12a) and obtain the net pressure force components

$$\begin{aligned} F_u^g &= -C_g^2 R_m \pi \,\mathrm{d}z \rho_1^c \cos\psi_u - C_g^2 R_m \pi \,\mathrm{d}z \rho_1^s \sin\psi_u - u\pi \,\mathrm{d}z C_g^2 (\rho_2^c \cos 2\psi_u + \rho_2^s \sin 2\psi_u) \\ F_\psi^g &= -C_g^2 R_m \pi \,\mathrm{d}z \rho_1^s \cos\psi_u + C_g^2 R_m \pi \,\mathrm{d}z \rho_1^c \sin\psi_u - u\pi \,\mathrm{d}z C_g^2 (\rho_2^s \cos 2\psi_u - \rho_2^c \sin 2\psi_u) \end{aligned} \tag{A14}$$

To calculate the net annulus drag force, we assume that the viscosity of the annulus $\mu(\theta)$ increases linearly with the volume fraction of magma in the deformed annulus as $\mu(\theta) = \mu_m(1 - \phi)$, where ϕ (see Appendix A3) is the gas volume fraction in the deformed annulus section. Using the expression (A28) for ϕ , $\mu(\theta)$ becomes

$$\mu(\theta) = \mu_m(1 - \phi_o)\left(1 + \frac{R_c - R_m}{U_m} u \cos\Delta\theta\right) \tag{A15}$$

where $U_m \equiv \frac{R_c^2 - R_m^2}{2R_m}$ (see Appendix A3). Substituting the expression for $\mu(\theta)$ into eqs (A11c) and (A11d) and integrating them according to eq. (A12b), we obtain the components of the net drag force

$$\begin{aligned} F_u^{\mathrm{ad}} &= -(\hat{u}\cdot\hat{v})\frac{R_m}{U_m}\pi \,\mathrm{d}z v\mu_m(1-\phi_o) \\ &\quad + 4(\hat{u}\cdot\hat{v})\frac{R_c - R_m - U_m}{U_m}\pi \,\mathrm{d}z v\mu_m(1-\phi_o)\left(\frac{\frac{3}{2} + \frac{1}{2}\frac{R_m}{R_c - R_m}}{1 + \sqrt{1 - \frac{u^2}{(R_c - R_m)^2}}} - \frac{3}{4}\right) \\ F_\psi^{\mathrm{ad}} &= \hat{z}\cdot(\hat{u}\times\hat{v})\frac{R_m}{U_m}\pi \,\mathrm{d}z v\mu_m(1-\phi_o) \\ &\quad - 4\hat{z}\cdot(\hat{u}\times\hat{v})\frac{R_c - R_m + U_m}{U_m}\pi \,\mathrm{d}z v\mu_m(1-\phi_o)\left(\frac{1}{4} - \frac{1}{\sqrt{1 - \frac{u^2}{(R_c - R_m)^2}}}\left(1 - \frac{\frac{3}{2} + \frac{1}{2}\frac{R_m}{R_c - R_m}}{1 + \sqrt{1 - \frac{u^2}{(R_c - R_m)^2}}}\right)\right) \end{aligned} \tag{A16}$$

The total pressure force and drag force are determined by eqs (A14) and (A16).

When the displacement u is also small compared with the width of the gas annulus such that $O(\frac{u^2}{(R_c - R_m)^2}) \sim 0$, eq. (A16) can be further reduced to its linear form

$$\begin{aligned} F_u^{\mathrm{ad}} &= -(\hat{u}.\hat{v})v(1-\phi_o)\mu_m\pi \,\mathrm{d}z\frac{R_m}{R_c - R_m} \\ F_\psi^{\mathrm{ad}} &= -\hat{z}\cdot(\hat{u}\times\hat{v})v(1-\phi_o)\mu_m\pi \,\mathrm{d}z\frac{R_m}{R_c - R_m} \end{aligned} \tag{A17}$$

The expressions for the total pressure force and drag force are determined by eqs (A14) and (A17) in cylindrical-polar coordinates, with the assumption of small displacement $u << R_c - R_m$. In Cartesian coordinates, the components of the forces can be obtained via

$$F_x^{g,\mathrm{ad}} = F_u^{g,\mathrm{ad}} \cos\psi_u - F_\psi^{g,\mathrm{ad}} \sin\psi_u, \qquad F_y^{g,\mathrm{ad}} = F_u^{g,\mathrm{ad}} \sin\psi_u + F_\psi^{g,\mathrm{ad}} \cos\psi_u \tag{A18}$$

where $\psi_u = \angle\frac{\hat{u}}{\hat{x}}$ is the polar angle of the displacement vector $\vec{u}$. Substituting eq. (A16) into eq. (A18), the components of the pressure and annulus drag force in the Cartesian coordinates become

$$\begin{aligned} F_x^g &= -C_g^2 R_m \pi \,\mathrm{d}z\rho_1^c - uC_g^2\pi \,\mathrm{d}z\left(\rho_2^c(\cos 2\psi_u \cos\psi_u + \sin 2\psi_u \sin\psi_u) + \rho_2^s(\sin 2\psi_u \cos\psi_u - \cos 2\psi_u \sin\psi_u)\right) \\ F_y^g &= -C_g^2 R_m \pi \,\mathrm{d}z\rho_1^s - uC_g^2\pi \,\mathrm{d}z\left(\rho_2^s(\cos 2\psi_u \cos\psi_u + \sin 2\psi_u \sin\psi_u) + \rho_2^c(\sin 2\psi_u \cos\psi_u - \cos 2\psi_u \sin\psi_u)\right) \\ F_x^{\mathrm{ad}} &= -v\left((\hat{u}\cdot\hat{v})\cos\psi_u - \hat{z}\cdot(\hat{u}\times\hat{v})\sin\psi_u\right)(1-\phi_o)\mu_m\pi \,\mathrm{d}z\frac{R_m}{R_c - R_m} \\ F_y^{\mathrm{ad}} &= -v\left((\hat{u}\cdot\hat{v})\sin\psi_u + \hat{z}\cdot(\hat{u}\times\hat{v})\cos\psi_u\right)(1-\phi_o)\mu_m\pi \,\mathrm{d}z\frac{R_m}{R_c - R_m} \end{aligned} \tag{A19}$$

in which the pressure force components can be further expressed as

$$\begin{aligned} F_x^g &= -C_g^2 R_m \pi \,\mathrm{d}z\rho_1^c - uC_g^2\pi \,\mathrm{d}z\rho_2^c \cos\psi_u - uC_g^2\pi \,\mathrm{d}z\rho_2^s \sin\psi_u \\ F_y^g &= -C_g^2 R_m \pi \,\mathrm{d}z\rho_1^s + uC_g^2\pi \,\mathrm{d}z\rho_2^c \sin\psi_u - uC_g^2\pi \,\mathrm{d}z\rho_2^s \cos\psi_u \end{aligned} \tag{A20}$$

and the drag force components can be further expressed using the relation (A5)

$$\begin{aligned} F_x^{\mathrm{ad}} &= -v\cos\psi_v(1-\phi_o)\mu_m\pi \,\mathrm{d}z\frac{R_m}{R_c - R_m} \\ F_y^{\mathrm{ad}} &= -v\sin\psi_v(1-\phi_o)\mu_m\pi \,\mathrm{d}z\frac{R_m}{R_c - R_m} \end{aligned} \tag{A21}$$

where $\psi_v = \angle^{\hat{v}}_{\hat{x}}$ is the polar angle of the velocity vector.

In Cartesian coordinates, the displacement of the magma column $\vec{u}$ has components u_x, u_y, and the velocity of the magma column $\vec{v}$ has components v_x, v_y, which can be calculated using their magnitudes u, v and polar angles ψ_u, ψ_v:

$$u_x = u\cos\psi_u, \quad u_y = u\sin\psi_u, \quad v_x = v\cos\psi_v, \quad v_y = v\sin\psi_v \tag{A22}$$

Substituting eq. (A22) into eqs (A20) and (A21), we finally obtain the expressions for the forces in Cartesian coordinates with the assumption of small displacement

$$\begin{aligned}
F_x^g &= -C_g^2 R_m \pi \,\mathrm{d}z \rho_1^c - C_g^2 \pi \,\mathrm{d}z \rho_2^c u_x - C_g^2 \pi \,\mathrm{d}z \rho_2^s u_y \\
F_y^g &= -C_g^2 R_m \pi \,\mathrm{d}z \rho_1^s + C_g^2 \pi \,\mathrm{d}z \rho_2^c u_y - C_g^2 \pi \,\mathrm{d}z \rho_2^s u_x \\
F_x^{\mathrm{ad}} &= -v_x(1-\phi_o)\mu_m \pi \,\mathrm{d}z \frac{R_m}{R_c - R_m} \\
F_y^{\mathrm{ad}} &= -v_y(1-\phi_o)\mu_m \pi \,\mathrm{d}z \frac{R_m}{R_c - R_m}
\end{aligned} \tag{A23}$$

which leads to the first three equations in eq. (3) after substituting $\frac{\partial \vec{u}}{\partial t}$ for $\vec{v}$.

Apart from the pressure force and the annulus drag force generated on the column–annulus interface, the magma column is also subjected to a viscous bending force $\vec{F}^{\mathrm{vb}}$, which is caused by the differential shear stresses acting on the upper and lower surfaces of the column section. The shear stress tensor $\boldsymbol{T}$ acts on a given horizontal surface intersecting the column such that

$$\boldsymbol{T}.\hat{z} = \mu_m \frac{\partial}{\partial z}\vec{v} \tag{A24}$$

where the horizontal velocity $\vec{v}$ is assumed to be uniform across the column interface but varying in vertical direction. The viscous bending force $\vec{F}^{\mathrm{vb}}$ can be obtained from the difference in $\boldsymbol{T}$ across the section's lower and upper surfaces

$$\vec{F}^{\mathrm{vb}} = [\mathbf{T}]|_z^{z+dz}\, \pi\, R_m^2 = \mu_m \pi\, R_m^2 \mathrm{d}z \frac{\partial^2}{\partial z^2}\frac{\partial \vec{u}}{\partial t} \tag{A25}$$

where πR_m^2 is the area of the upper and lower surfaces. Eq. (A25) leads to the last equation in eq. (3).

A3 Gas flux dynamics

The volume of the annulus segment spanned by the angular increment $\mathrm{d}\theta$ (see Fig. A1) and vertical increment $\mathrm{d}z$ is $\mathrm{d}V = \mathrm{d}z \int_{r_m}^{R_c} r\,\mathrm{d}\theta\,\mathrm{d}r$. Under the assumption of small displacement, $\mathrm{d}V$ is further expressed using the expression for r_m in eq. (A1):

$$\mathrm{d}V = \mathrm{d}V_o[1 - \frac{u}{U_m}\cos\Delta\theta] \tag{A26}$$

where $U_m \equiv \frac{R_c^2 - R_m^2}{2R_m}$, and $\mathrm{d}V_o = \frac{1}{2}(R_c^2 - R_m^2)\mathrm{d}\theta\mathrm{d}z$ is the volume of the undeformed annulus section. The volume of magma in the undeformed annulus section is $\mathrm{d}V_m = \mathrm{d}V_o(1-\phi_o)$, where ϕ_o is the undisturbed gas volume fraction. We assume that the magma matrix is incompressible due to the high compressibility of the gas phase, hence $\mathrm{d}V_m$ is constant. In the deformed annulus section with total volume $\mathrm{d}V$, the gas volume $\mathrm{d}V_g = \mathrm{d}V - \mathrm{d}V_m = \varphi(\theta)\mathrm{d}V_o$, where φ, defined as $\mathrm{d}V_g/\mathrm{d}V_o$, is

$$\varphi(\theta) = \phi_o - \frac{u}{U_m}\cos\Delta\theta \tag{A27}$$

The gas volume fraction in the deformed annulus section $\phi(\theta) = \mathrm{d}V_g/\mathrm{d}V$ is, to first order of u:

$$\phi(\theta) = \phi_o - (1-\phi_o)\frac{u}{U_m}\cos\Delta\theta \tag{A28}$$

Using the relation $\Delta\theta = \theta - \psi_u$ and the relation (A22), we re-express eqs (A28) and (A27) as

$$\varphi(\theta) = \phi_o - \frac{u_x\cos\theta + u_y\sin\theta}{U_m} \tag{A29a}$$

$$\phi(\theta) = \phi_o - (1-\phi_o)\frac{u_x\cos\theta + u_y\sin\theta}{U_m} \tag{A29b}$$

which leads to eq. (6) in the main text. The conservation of mass in the deformed annulus section is expressed as

$$\frac{\partial(\rho\varphi)}{\partial t} + \frac{\partial(\rho\varphi w)}{\partial z} = 0 \tag{A30}$$

where $\rho = \rho(\theta, t, z)$ and $w = w(\theta, t, z)$ are the gas density and velocity in the annulus. The equation of motion for the gas flux can be achieved by analysing the forces on both the gas and the magma phase following (Bercovici *et al.* 2013), which yield

$$\rho\phi\left(\frac{\partial w}{\partial t} + w\frac{\partial w}{\partial z}\right) = -C_g^2\frac{\partial \rho}{\partial z} - ((1-\phi)\rho_m + \phi\rho)\,g \tag{A31}$$

where ρ_m is the density of the magma. The first term on the right-hand side of eq. (A31) denotes the pressure gradient force, which follows the assumption of a constant isothermal gas sound speed C_g and the ideal gas law $P(\theta) = C_g^2\rho(\theta)$. The second term on the right-hand side of eq. (A31) is the gravitational force acting on the mixture of gas and magma within the annulus section, which results from combining the equations of motion of the gas and magma phases. Although the permeability in the gas annulus is not explicitly incorporated in eq. (A31), it is implicitly required for the Darcy drag of the porous gas flows [for detailed derivation, refer to Bercovici *et al.* (2013)].

Given azimuthal periodicity, the gas density and velocity can be expressed as discrete Fourier series

$$\rho(\theta) = \rho_o + \sum_{m=1}^{\infty}\left(\rho_m^c \cos m\theta + \rho_m^s \sin m\theta\right) \tag{A32a}$$

$$w(\theta) = W_o + \sum_{m=1}^{\infty}\left(w_m^c \cos m\theta + w_m^s \sin m\theta\right) \tag{A32b}$$

where ρ_n^c, w_n^c, ρ_n^s and w_n^s ($n = 1, 2, 3, \ldots$) are the Fourier coefficients that vary with time t and height z.

APPENDIX B: LINEAR STABILITY ANALYSIS

B1 Dimensionless linear equations for perturbations

We select the annulus' width $R_c - R_m$ for the length scale, $(R_c - R_m)/C_g$ for a timescale and the unperturbed gas density ρ_o as the density scale to non-dimensionalize the governing equations. The dimensionless governing equations corresponding to eqs (A23), (A30) and (A31) become

$$\begin{aligned}
&\frac{\partial(\rho\varphi)}{\partial t} + \frac{\partial(\rho\varphi w)}{\partial z} = 0\\
&\rho\phi\left(\frac{\partial w}{\partial t} + w\frac{\partial w}{\partial z}\right) = -\frac{\partial \rho}{\partial z} - \gamma\left(\beta(1-\phi) + \rho\phi\right)\\
&\frac{\partial^2 u_x}{\partial t^2} = -\frac{\lambda}{\beta}\rho_1^c - \frac{\lambda^2}{\beta}(\rho_2^c u_x + \rho_2^s u_y) + \eta\frac{\partial^3 u_x}{\partial z^2 \partial t} - (1-\phi_o)\eta\lambda\frac{\partial u_x}{\partial t}\\
&\frac{\partial^2 u_y}{\partial t^2} = -\frac{\lambda}{\beta}\rho_1^s + \frac{\lambda^2}{\beta}(\rho_2^c u_y - \rho_2^s u_x) + \eta\frac{\partial^3 u_y}{\partial z^2 \partial t} - (1-\phi_o)\eta\lambda\frac{\partial u_y}{\partial t}
\end{aligned} \tag{B1}$$

where ρ, w and $u_{x,y}$ have been normalized by their respective scales. The dimensionless constants are defined as

$$\beta = \rho_m/\rho_o, \quad \lambda = \frac{R_c - R_m}{R_m}, \quad \eta = \frac{\mu_m}{\rho_m C_g (R_c - R_m)}, \quad \gamma = \frac{(R_c - R_m)g}{C_g^2} \tag{B2}$$

The dimensionless number β is the ratio of magma and gas density, λ is a measure of annulus thickness relative to the column width, η measures the competition between the viscous damping and gas spring forces and γ measures the competition between hydrostatic pressure and gas pressure. In the rest of our study, we assume $g = \gamma = 0$ following Bercovici *et al.* (2013).

A steady-state solution for eq. (B1) can be readily found, which corresponds to the undisturbed system with a uniform gas velocity W_o. The steady-state solution for the displacement is $u_{x,y}^{(0)} = 0$. The steady solution for the gas density is $\rho^{(0)} = 1$ and for the gas velocity $w^{(0)} = W_o/C_g$. Both the solutions for the gas density and gas velocity are uniform across the annulus and independent of θ. Therefore, the corresponding Fourier coefficients are $\rho_n^{c,(0)} = \rho_n^{s,(0)} = w_n^{c,(0)} = w_n^{s,(0)} = 0$.

We introduce a small perturbation to the system, which leads to the new solutions of $u_x = \epsilon u_x^{(1)}$, $u_y = \epsilon u_y^{(1)}$, $\rho = 1 + \epsilon\sum_n^{\infty}\left(\rho_n^{c,(1)}\cos n\theta + \rho_n^{s,(1)}\sin n\theta\right)$ and $w = M + \epsilon\sum_n^{\infty}\left(w_n^{c,(1)}\cos n\theta + w_n^{s,(1)}\sin n\theta\right)$, where $\epsilon \ll 1$, $M = W_o/C_g$ is defined as a gas injection Mach number and the subscript $^{(1)}$ indicates the first-order perturbations. We substitute the perturbation solutions into eq. (B1), take the first order of ϵ, and obtain six linearized equations (wherein the superscript '$^{(1)}$ 'is dropped):

$$\begin{aligned}
(\frac{\partial}{\partial t} + M\frac{\partial}{\partial z})(\phi_o\rho_1^{c,s} - \zeta u_{x,y}) + \phi_o\frac{\partial w_1^{c,s}}{\partial z} &= 0\\
\phi_o(\frac{\partial}{\partial t} + M\frac{\partial}{\partial z})w_1^{c,s} + \frac{\partial \rho_1^{c,s}}{\partial z} &= 0\\
\frac{\partial^2 u_{x,y}}{\partial t^2} + \frac{\lambda}{\beta}\rho_1^{c,s} - \eta\frac{\partial^3 u_{x,y}}{\partial t \partial z^2} + (1-\phi_o)\eta\lambda\frac{\partial u_{x,y}}{\partial t} &= 0
\end{aligned} \tag{B3}$$

where

$$\zeta = (R_c - R_m)/U_m = 2/(\lambda + 2) \tag{B4}$$

With the linear approximation, the evolution of higher degree components ($m > 1$) in gas density and velocity are governed by the sound-wave equations, which are decoupled from the motion of the magma column. Because λ is small (assuming thin annulus), the contributions from

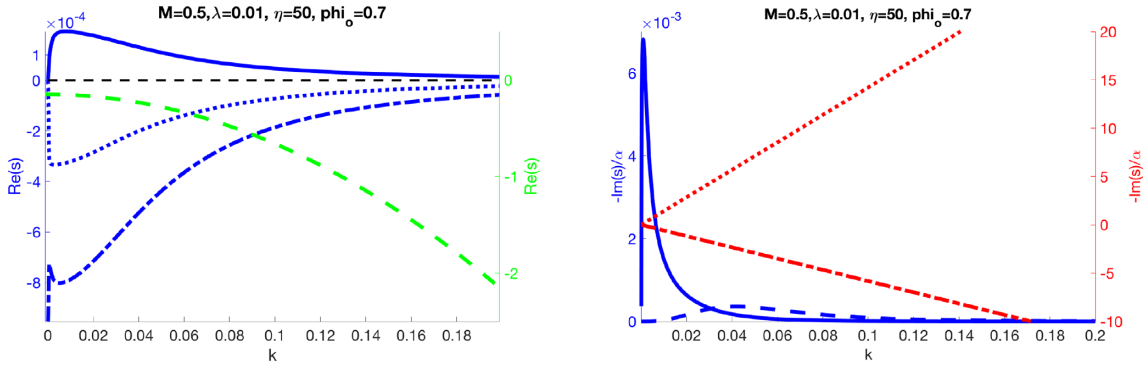

(a) (b)

Figure B1. Complex growth rate s according to dispersion relation resulting from the solution to eq. (B6). Frame (a) shows Re(s) as a function of wavenumber k for all four roots of eq. (B6). Values of the three blue curves are shown by the y-axis on the left; values of the green curve are shown by the y-axis on the right. Frame (b) shows $-$Im(s) as a function of wavenumber k for the four roots. The oscillation frequency is normalized by the inviscid oscillation frequency α generated by an impermeable annulus, as defined in eq. (B12). Two blue curves have small oscillation frequencies, whose values are shown on the y-axis on the left; and two red curves have high oscillation frequencies, whose values are shown on the y-axis on the right.

the higher degree components to the non-linear evolutions of the magma column's motions are limited due to higher powers in λ in eq. (B1). Therefore, to study the interactions between the gas flux and the wagging motion, and also assuming a thin vesicular annulus, we focus on the lowest degree components $\rho_1^{c,s}$ and $w_1^{c,s}$ in the rest of our study.

The first-order perturbations governed by eq. (B3) indicate that the evolution of the gas flux with even symmetry (ρ_1^c, w_1^c) is coupled to the evolution of u_x , while the evolution of gas flux with odd symmetry (ρ_1^s, w_1^s) is coupled with u_y only. As a result, the evolution of (ρ_1^c, w_1^c, u_x) is independent from the evolution of (ρ_1^s, w_1^s, u_y) and the evolution of the column displacement $\vec{u} = \epsilon u_x \hat{x} + \epsilon u_y \hat{y}$ is the superposition of two 1-D displacements in orthogonal directions. Note that these relations are only true in the linear approximation when the displacement is very small.

B2 Linear stability analysis and dispersion relation

The solution for eq. (B3) can be expressed as a superposition of propagating waves

$$u_{x,y} = \sum_k \widehat{u_{x,y}} e^{ikz+st} \quad \rho_1^{c,s} = \sum_k \widehat{\rho_1^{c,s}} e^{ikz+st} \quad w_1^{c,s} = \sum_k \widehat{w_1^{c,s}} e^{ikz+st} \tag{B5}$$

where $\widehat{u_{x,y}}$, $\widehat{\rho_1^{c,s}}$ and $\widehat{w_1^{c,s}}$ are complex amplitudes for the Fourier modes, and the complex growth rate s is a function of wavenumber k. Substituting the wave-like solutions (B5) into (B3), we obtain the characteristic equation for s

$$s^2 + \frac{\phi_o \alpha^2 (s+ikM)^2}{k^2 + \phi_o (s+ikM)^2} + \eta \left(k^2 + (1-\phi_o)\lambda\right) s = 0 \tag{B6}$$

the solution for which is the dispersion relation $s(k)$. Taking the real and imaginary components separately, the characteristic eq. (B6) leads to

$$\sigma^2 - \omega^2 + \phi_o \alpha^2 \mathrm{Re}\left(\frac{(s+ikM)^2}{k^2 + \phi_o (s+ikM)^2}\right) + \eta \left(k^2 + (1-\phi_o)\lambda\right) \sigma = 0 \tag{B7a}$$

$$-2(\sigma\omega) + \mathrm{Im}\left(\frac{(s+ikM)^2}{k^2 + \phi_o (s+ikM)^2}\right) - \eta \left(k^2 + (1-\phi_o)\lambda\right) \omega = 0 \tag{B7b}$$

where $\sigma(k)$ and $\omega(k)$ are real numbers defined by

$$\sigma = \mathrm{Re}(s), \qquad \omega = -\mathrm{Im}(s) \tag{B8}$$

For each wavenumber k, there are four distinct roots for eq. (B6), three of which are stable with Re(s) < 0 (Fig. B1a, dashed and dotted curves in blue and green), and one unstable with Re(s) > 0 (Fig. B1a, blue solid curve). Both the unstable root and the rapid-decay root correspond to low-frequency oscillations (Fig. B1b, blue curves), whose periods are much longer than that of the fundamental oscillation frequency α, defined in eq. (B12), which corresponds to $\sim$ 1 Hz tremor (Jellinek & Bercovici 2011; Bercovici *et al.* 2013). The two slower decay roots, which behave similar to up- and down-propagating sound waves, have high-frequency oscillations (Fig. B1b, red curves). Similar findings were first discovered by Bercovici *et al.* (2013) in their 2-D magma wagging model, in which the unstable root was recognized as a consequence of Bernoulli effect. Here, the Bernoulli effect induces an instability in three dimensions, driving instabilities in both $\hat{x}$ and $\hat{y}$ components of the displacement and serves as an excitation mechanism for the 3-D whirling motion. Therefore, we will refer to the perturbation with Re(s) > 0 as the Bernoulli perturbation, as it is a consequence of the Bernoulli effect.

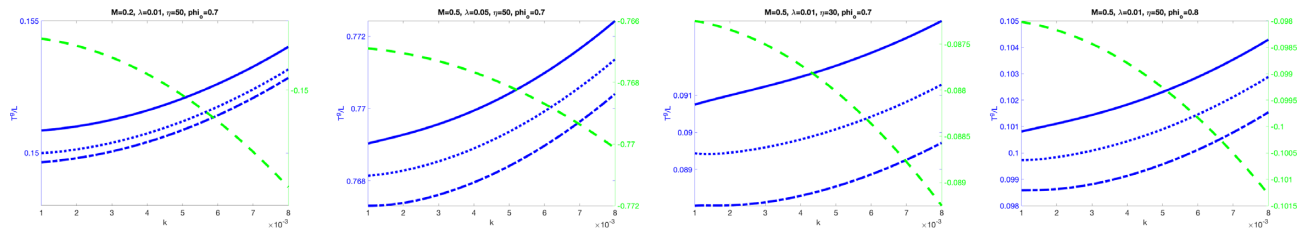

(a) (b) (c) (d)

Figure B2. Gas torques associated to all four roots as function of wavenumber, with variations in system parameters M, λ, η and ϕ_o.

It is worth noting that, if the system has an impermeable gas annulus as assumed in previous models (Jellinek & Bercovici 2011; Liao *et al.* 2018), the mass of gas phase in any deformed annulus section conserved, thus $\rho \mathrm{d}V_g = \rho_o \mathrm{d}V_o \phi_o$ (see Appendix A3). Using the expression (A27) for φ, the gas density in the impermeable annulus becomes

$$\rho(\theta) = \rho_o \phi_o / \varphi = \rho_o + \frac{\rho_o}{\phi_o U_m} u \cos \Delta\theta \tag{B9}$$

Comparing eq. (B9) with the alternative expression (A32a) for $\rho(\theta)$ using its Fourier modes, we observe that the Fourier coefficients in eq. (A32a) must satisfy

$$\rho_1^c = \frac{\rho_o u_x}{U_m \phi_o}, \quad \rho_1^s = \frac{\rho_o u_y}{U_m \phi_o}$$

and

$$\rho_n^c = \rho_n^s = 0 \quad (n > 1)$$

After being normalized by the density scale ρ_o and length scale $R_c - R_m$, the dimensionless density perturbations become

$$\rho_1^c = \zeta u_x / \phi_o, \quad \rho_1^s = \zeta u_y / \phi_o \tag{B10}$$

which contribute to the restoring force in eq. (A23). Substituting the above relation to eq. (B3), the governing equations for the first-order perturbation in the magma column's displacement becomes

$$\frac{\partial^2 u_{x,y}}{\partial t^2} + \alpha^2 u_{x,y} = \eta \frac{\partial^3 u_{x,y}}{\partial t \partial z^2} - (1 - \phi_o)\eta\lambda \frac{\partial u_{x,y}}{\partial t} \tag{B11}$$

where

$$\alpha = \sqrt{\frac{\lambda\zeta}{\beta\phi_o}} \tag{B12}$$

corresponds to the fundamental oscillation frequency. Substituting the waveform solutions (B5) into (B11), the characteristic equation becomes

$$s = -\frac{1}{2}\left(k^2 + (1 - \phi_o)\lambda\right)\eta \pm \alpha i \sqrt{1 - \frac{\left(k^2 + (1 - \phi_o)\lambda\right)^2 \eta^2}{4}} \tag{B13}$$

which in the limit of small wavenumber k and thin annulus width λ becomes

$$s = -\frac{1}{2}\left(k^2 + (1 - \phi_o)\lambda\right)\eta \pm \alpha i$$

which corresponds to a damped oscillation with frequency α. Substituting the definitions of the dimensionless numbers eqs (B2) and (B4) into eq. (B12), the dimensional oscillation frequency for the impermeable annulus becomes $\sqrt{\frac{2\rho_o C_g^2}{\phi_o \rho_m (R_c^2 - R_m^2)}}$, recovering the fundamental frequency in the previous models with impermeable gas annulus (Jellinek & Bercovici 2011; Liao *et al.* 2018).

B3 Gas density response factor and its link to growing instabilities

The Fourier coefficients for the gas density $\widehat{\rho_1^{c,s}}$ defined in eq. (B5) can be expressed as a response to the Fourier coefficient in the magma column displacement $\widehat{u_{x,y}}$

$$\widehat{\rho_1^{c,s}} = \widetilde{\Theta}\widehat{u_{x,y}} \tag{B14}$$

where $\widetilde{\Theta}$ is defined as the response factor between gas density and column displacement and is calculated by substituting eqs (B5) and (B6) into (B3)

$$\widetilde{\Theta} = \frac{\zeta(s + Mki)^2}{\phi_o(s + Mki)^2 + k^2}, \tag{B15}$$

The real and imaginary parts of the gas density response factor (B15) can be expressed separately as

$$\mathrm{Re}\left(\widetilde{\Theta}\right) = \zeta \mathrm{Re}\left(\frac{(s+Mki)^2}{\phi_o(s+Mki)^2+k^2}\right) \qquad \mathrm{Im}\left(\widetilde{\Theta}\right) = \zeta \mathrm{Im}\left(\frac{(s+Mki)^2}{\phi_o(s+Mki)^2+k^2}\right) \tag{B16}$$

Substituting eqs (B16) into (B7), we obtain

$$\sigma^2 - \omega^2 + \phi_o \tfrac{\alpha^2}{\zeta} \mathrm{Re}\left(\widetilde{\Theta}\right) + \eta\left(k^2 + (1-\phi_o)\lambda\right)\sigma = 0 \tag{B17a}$$

$$-2(\sigma\omega) + \phi_o \tfrac{\alpha^2}{\zeta} \mathrm{Im}\left(\widetilde{\Theta}\right) - \eta\left(k^2 + (1-\phi_o)\lambda\right)\omega = 0 \tag{B17b}$$

$$-(\sigma^2+\omega^2) + \phi_o \tfrac{\alpha^2}{\zeta}\left(\mathrm{Re}(\widetilde{\Theta}) + \sigma \tfrac{\mathrm{Im}(\widetilde{\Theta})}{\omega}\right) = 0 \tag{B17c}$$

where eq. (B17c) is obtained by summing up the products of eq. (B17a) multiplied by ω and eq. (B17b) multiplied by σ.

Substituting the expression for α in eqs (B12) into (B17 b) leads to the relation between the growth rate σ and the gas response factor

$$\sigma = \frac{\mathrm{Im}(\Theta)\lambda}{2\omega\beta} - \frac{\eta k^2}{2} - \frac{(1-\phi_o)\lambda\eta}{2} \tag{B18}$$

In contrast, the growth rate determined by eq. (B13) for an impermeable annulus is

$$\sigma = \mathrm{Re}(s) = -\frac{\eta k^2}{2} - \frac{(1-\phi_o)\lambda\eta}{2} \tag{B19}$$

which is always negative. Comparison between eqs (B18) and (B19) suggests that the Bernoulli perturbation, for which $\sigma > 0$, is linked to the variation in gas density and exists only when the annulus is permeable.

B4 Expressions of linear perturbations in real space

The displacement in real space can be obtained by taking the real part of eq. (B5). When the system is dominated by a single root (e.g. when time progressed long enough such that the decay roots are damped out, the Bernoulli perturbation dominates) with angular frequency $s = \sigma - i\omega$ and wavenumber k, the displacement components u_x and u_y at height z is

$$\begin{aligned}
u_{x,y}(t,z) &= \mathrm{Re}\left(\widehat{u_{x,y}} e^{ikz+(\sigma-i\omega)t}\right) \\
&= \mathrm{Re}\left(\left(\mathrm{Re}(\widehat{u_{x,y}}) + i\,\mathrm{Im}(\widehat{u_{x,y}})\right)(\cos kz + i\sin kz)(\cos\omega t - i\sin\omega t)\right) e^{\sigma t} \\
&= \left(\mathrm{Re}(\widehat{u_{x,y}})\cos kz\cos\omega t + \mathrm{Re}(\widehat{u_{x,y}})\sin kz\sin\omega t + \mathrm{Im}(\widehat{u_{x,y}})\cos kz\sin\omega t - \mathrm{Im}(\widehat{u_{x,y}})\sin kz\cos\omega t\right) e^{\sigma t} \\
&= \left(\mathrm{Re}(\widehat{u_{x,y}})\cos\omega t + \mathrm{Im}(\widehat{u_{x,y}})\sin\omega t\right)\cos kz e^{\sigma t} + \left(\mathrm{Re}(\widehat{u_{x,y}})\sin\omega t - \mathrm{Im}(\widehat{u_{x,y}})\cos\omega t\right)\sin kz e^{\sigma t} \\
&= |\widehat{u_{x,y}}|\cos\left(\omega t - \tan^{-1}\left(\frac{\mathrm{Im}(\widehat{u_{x,y}})}{\mathrm{Re}(\widehat{u_{x,y}})}\right)\right)\cos kz e^{\sigma t} + |\widehat{u_{x,y}}|\sin\left(\omega t - \tan^{-1}\left(\frac{\mathrm{Im}(\widehat{u_{x,y}})}{\mathrm{Re}(\widehat{u_{x,y}})}\right)\right)\sin kz e^{\sigma t} \\
&= |\widehat{u_{x,y}}|\cos\left(\omega(t-\tau^u_{x,y}) - kz\right) e^{\sigma t}
\end{aligned} \tag{B20}$$

where $|\widehat{u_{x,y}}|$ and $\tau^u_{x,y}$ are defined as

$$|\widehat{u_{x,y}}| = \sqrt{\mathrm{Re}(\widehat{u_{x,y}})^2 + \mathrm{Im}(\widehat{u_{x,y}})^2}, \qquad \tau^u_{x,y} = \tan^{-1}\left(\frac{\mathrm{Im}(\widehat{u_{x,y}})}{\mathrm{Re}(\widehat{u_{x,y}})}\right)/\omega \tag{B21}$$

The amplitudes $|\widehat{u_x}|$ and $|\widehat{u_y}|$ indicate the initial values of the displacement components u_x and u_y, and the time-shifts τ^u_x and τ^u_y are determined by the initial phases of the oscillatory parts in u_x and u_y, respectively. The gas density ρ_c and ρ_s can be obtained from eq. (B5) following similar derivation as eq. (B20), finally leading to the expressions of a single root in real space and time

$$u_{x,y} = \mathrm{Re}\left(\widehat{u_{x,y}} e^{ikz+st}\right) = |\widehat{u_{x,y}}|\cos\left(\omega(t-\tau^u_{x,y}) - kz\right) e^{\sigma t} \tag{B22a}$$

$$\rho_1^{c,s} = |\Theta||u_{x,y}|\cos(\omega(t-\tau^u_{x,y}-\tau^\rho) - kz)e^{\sigma t} \tag{B22b}$$

where

$$|\Theta| = \sqrt{\mathrm{Re}(\widetilde{\Theta})^2 + \mathrm{Im}(\widetilde{\Theta})^2} \quad \tau^\rho = \frac{1}{\omega}\tan^{-1}\left(\frac{\mathrm{Im}(\widetilde{\Theta})}{\mathrm{Re}(\widetilde{\Theta})}\right) \tag{B23}$$

Take the time derivative of eq. (B22a), we obtain the velocity components $v_{x,y} = \partial u_{x,y}/\partial t$:

$$\begin{aligned}
v_{x,y} &= \sigma|\widehat{u_{x,y}}|\cos\left(\omega(t-\tau^u_{x,y}) - kz\right) e^{\sigma t} - \omega|\widehat{u_{x,y}}|\sin\left(\omega(t-\tau^u_{x,y}) - kz\right) e^{\sigma t} \\
&= \sigma u_{x,y} - \omega|\widehat{u_{x,y}}|\sin\left(\omega(t-\tau^u_{x,y}) - kz\right) e^{\sigma t}
\end{aligned} \tag{B24}$$

The responses of gas density components $\rho_{c,s}$ can also be expressed in terms of the displacement and velocity. Rewrite the time-shift τ^{ρ} in eq. (B23) as

$$\cos\omega\tau^{\rho} = \frac{\mathrm{Re}(\widetilde{\Theta})}{\sqrt{\mathrm{Re}(\widetilde{\Theta})^2 + \mathrm{Im}(\widetilde{\Theta})^2}}, \quad \sin\omega\tau^{\rho} = \frac{\mathrm{Im}(\widetilde{\Theta})}{\sqrt{\mathrm{Re}(\widetilde{\Theta})^2 + \mathrm{Im}(\widetilde{\Theta})^2}}, \quad |\widetilde{\Theta}| = \sqrt{\mathrm{Re}(\widetilde{\Theta})^2 + \mathrm{Im}(\widetilde{\Theta})^2}$$

and substitute it into eq. (B22b), we expand the density components as

$$\begin{aligned}\rho_1^{c,s} &= |\widetilde{\Theta}||\widehat{u_{x,y}}|\left(\cos\left(\omega(t-\tau^u_{x,y})-kz\right)\cos\omega\tau^{\rho} + \sin\left(\omega(t-\tau^u_{x,y})-kz\right)\sin\omega\tau^{\rho}\right)e^{\sigma t}\\ &= |\widehat{u_{x,y}}|e^{\sigma t}\mathrm{Re}(\widetilde{\Theta})\cos\left(\omega(t-\tau^u_{x,y})-kz\right) + |\widehat{u_{x,y}}|e^{\sigma t}\mathrm{Im}(\widetilde{\Theta})\sin\left(\omega(t-\tau^u_{x,y})-kz\right)\\ &= \mathrm{Re}(\widetilde{\Theta})u_{x,y} + |\widehat{u_{x,y}}|e^{\sigma t}\mathrm{Im}(\widetilde{\Theta})\sin\left(\omega(t-\tau^u_{x,y})-kz\right)\end{aligned} \tag{B25}$$

Substituting eqs (B22a) and (B24) into (B25), $\rho_1^{c,s}$ then become

$$\rho_1^{c} = \left(\mathrm{Re}(\widetilde{\Theta}) + \frac{\mathrm{Im}(\widetilde{\Theta})\sigma}{\omega}\right)u_x - \frac{\mathrm{Im}(\widetilde{\Theta})}{\omega}v_x \tag{B26a}$$

$$\rho_1^{s} = \left(\mathrm{Re}(\widetilde{\Theta}) + \frac{\mathrm{Im}(\widetilde{\Theta})\sigma}{\omega}\right)u_y - \frac{\mathrm{Im}(\widetilde{\Theta})}{\omega}v_y \tag{B26b}$$

B5 Energy and angular momentum of the Bernoulli perturbation

B5.1 Definitions of linear forces

Observing the linear evolution equation for the displacement of the magma column in eq. (B3)

$$\frac{\partial^2 u_{x,y}}{\partial t^2} = -\frac{\lambda}{\beta}\rho_1^{c,s} + \eta\frac{\partial^3 u_{x,y}}{\partial t\partial z^2} - (1-\phi_o)\eta\lambda\frac{\partial u_{x,y}}{\partial t} \tag{B27}$$

We can define three dimensionless forces from the above equation

$$\vec{F}^{g} = -\frac{\lambda}{\beta}\left(\rho_1^{c}\hat{x} + \rho_1^{s}\hat{y}\right) \tag{B28a}$$

$$\vec{F}^{\mathrm{vb}} = \eta\frac{\partial^2}{\partial z^2}\frac{\partial\vec{u}}{\partial t} \tag{B28b}$$

$$\vec{F}^{\mathrm{ad}} = -(1-\phi_o)\eta\lambda\frac{\partial\vec{u}}{\partial t} \tag{B28c}$$

in which $\vec{F}^{\mathrm{vb}}$ and $\vec{F}^{\mathrm{ad}}$ correspond to the viscous bending force on the deformed magma column and the annulus drag force at the column–annulus interface, respectively; and $\vec{F}^{g}$ is the gas pressure force for the linear perturbations. Using these forces, the dimensionless evolution equation for the linear perturbations can be expressed as

$$\frac{\partial^2\vec{u}}{\partial t^2} = \vec{F}^{g} + \vec{F}^{\mathrm{vb}} + \vec{F}^{\mathrm{ad}} \tag{B29}$$

When the system is dominated by perturbation with a single growth rate and wavenumber, the forces can be expressed using the magma column's displacement $\vec{u}$ and velocity $\vec{v} = \partial\vec{u}/\partial t$ by substituting eqs (B5) and (B26) into (B28)

$$\begin{aligned}\vec{F}^{g} &= -\frac{\lambda}{\beta}\left(\frac{\mathrm{Im}(\widetilde{\Theta})\sigma}{\omega} + \mathrm{Re}(\widetilde{\Theta})\right)\vec{u} + \frac{\lambda}{\beta}\frac{\mathrm{Im}(\widetilde{\Theta})}{\omega}\vec{v}\\ \vec{F}^{\mathrm{vb}} &= -\eta k^2\vec{v}\\ \vec{F}^{\mathrm{ad}} &= -(1-\phi_o)\eta\lambda\vec{v}\end{aligned} \tag{B30}$$

where $\widetilde{\Theta}$ is calculated according to eq. (B15). It is worth noting that when the gas annulus is impermeable, the density perturbations are determined by eq. (B10), in which case eq. (B28a) reduces to

$$\vec{F}^{g} = -\frac{\lambda\zeta}{\beta\phi_o}\vec{u} \tag{B31}$$

which is always parallel with the displacement $\vec{u}$ of the magma column.

B5.2 Angular momentum and torques

We define the dimensionless angular momentum $\vec{L} = \vec{u} \times \vec{v}$ and the dimensionless torques as $\vec{\mathcal{T}}^{g,\mathrm{vb,ad}} \equiv \vec{u} \times \vec{F}^{g,\mathrm{vb,ad}}$, which are further expressed after taking the cross product of $\vec{u}$ and eq. (B30)

$$\vec{\mathcal{T}}^{\mathrm{vb}} = -\eta k^2 \vec{L}, \qquad \vec{\mathcal{T}}^{\mathrm{ad}} = -(1-\phi_o)\lambda\eta\vec{L}, \qquad \vec{\mathcal{T}}^{g} = \frac{\mathrm{Im}(\Theta)\lambda}{\omega\beta}\vec{L} \tag{B32}$$

The evolution of the angular momentum becomes

$$\frac{\partial \vec{L}}{\partial t} = \frac{\partial \vec{u}}{\partial t} \times \frac{\partial \vec{u}}{\partial t} + \vec{u} \times \frac{\partial^2 \vec{u}}{\partial t^2} = \vec{u} \times \frac{\partial^2 \vec{u}}{\partial t^2} = \vec{\mathcal{T}}^{\mathrm{vb}} + \vec{\mathcal{T}}^{\mathrm{ad}} + \vec{\mathcal{T}}^{g} \tag{B33}$$

A total torque $\vec{\mathcal{T}}^{\mathrm{tot}} = \vec{\mathcal{T}}^{\mathrm{vb}} + \vec{\mathcal{T}}^{\mathrm{ad}} + \vec{\mathcal{T}}^{g}$ can be further calculated using the relation in eq. (B18)

$$\vec{\mathcal{T}}^{\mathrm{tot}} = \left(\frac{\mathrm{Im}(\Theta)\lambda}{\omega\beta} - \eta k^2 - (1-\phi_o)\lambda\eta\right)\vec{L} = 2\sigma\vec{L} \tag{B34}$$

For a complex growth rate, the angular momentum of the magma column $\vec{L} = \vec{u} \times \vec{v} = L\hat{z}$ has non-zero component in the $\hat{z}$ direction, where the amplitude L can be expanded using eqs (B22a) and (B24)

$$\begin{aligned}
L &= u_x v_y - u_y v_x \\
&= |\widehat{u_x}\widehat{u_y}|e^{2\sigma t}\left(\sigma\cos\left(\omega(t-\tau_y^u)-kz\right)\cos\left(\omega(t-\tau_x^u)-kz\right) - \omega\sin\left(\omega(t-\tau_y^u)-kz\right)\cos\left(\omega(t-\tau_x^u)-kz\right)\right) \\
&\quad -|\widehat{u_x}\widehat{u_y}|e^{2\sigma t}\left(\sigma\cos\left(\omega(t-\tau_x^u)-kz\right)\cos\left(\omega(t-\tau_y^u)-kz\right) - \omega\sin\left(\omega(t-\tau_x^u)-kz\right)\cos\left(\omega(t-\tau_y^u)-kz\right)\right) \\
&= |\widehat{u_x}\widehat{u_y}|\omega e^{2\sigma t}\left(\sin\left(\omega(t-\tau_x^u)-kz\right)\cos\left(\omega(t-\tau_y^u)-kz\right) - \sin\left(\omega(t-\tau_y^u)-kz\right)\cos\left(\omega(t-\tau_x^u)-kz\right)\right) \\
&= |\widehat{u_x}\widehat{u_y}|\omega e^{2\sigma t}\sin\left(\left(\omega(t-\tau_x^u)-kz\right)-\left(\omega(t-\tau_y^u)-kz\right)\right) \\
&= |\widehat{u_x}\widehat{u_y}|\omega e^{2\sigma t}\sin\left(\omega(\tau_y^u-\tau_x^u)\right)
\end{aligned} \tag{B35}$$

We observe from eq. (B35) that if the relation between the two Fourier coefficients satisfies $\tau_x^u - \tau_y^u = n\pi$ ($n = 0, 1, 2, \ldots$), then the displacement components u_x and u_y determined by eq. (B22a) are always proportional to each other, which corresponds to 2-D motion, in which case the angular momentum is zero. If the motion is 3-D but the gas annulus is impermeable [the case in Liao *et al.* (2018)], $\vec{F}^{g} \parallel \vec{u}$ according to eq. (B31), causing the torque $\vec{\mathcal{T}}^{g} = \vec{u} \times \vec{F}^{g}$ to vanish. In this condition, the angular momentum decays under the negative viscous torques. When the motion is 3-D and the annulus is permeable, the gas torque has a finite value. We observe from eq. (B32) that $\vec{\mathcal{T}}^{\mathrm{vb}}$ and $\vec{\mathcal{T}}^{\mathrm{ad}}$ are always in the opposite direction of $\vec{L}$ (i.e. when rotation is clockwise, the torques are counterclockwise, and vice versa), hence contribute to decreasing $\vec{L}$. In contrast, the sign of $\vec{\mathcal{T}}^{g}$ is positive for three out of the four roots of s for any given wavenumber (see Fig. 2 a and Fig. B2). However, it is only for the unstable root that $\vec{\mathcal{T}}^{g}$ is large enough to counter the two negative torques $\vec{\mathcal{T}}^{\mathrm{ad,vb}}$, which yield a positive net torque $\vec{\mathcal{T}}^{\mathrm{tot}}$ indicated in eq. (B34). Therefore, we refer to the gas torque $\vec{\mathcal{T}}^{g}$ of the Bernoulli perturbation as the Bernoulli torque. The gas torques as functions of wavenumber k remain qualitatively similar, despite variations in the system's parameters such as magma viscosity, gas injection velocity, annulus width and porosity. As the Bernoulli effect depends on the velocity of the gas flows, the Bernoulli torque increases with increasing gas injection velocity (see Fig. 2b).

B5.3 Energy and power sources

To define an energy for the wagging magma column, we first observe the acceleration of the magma column in eq. (B29), which can be expanded using the displacement and velocity of the magma column using eq. (B30) when the system is dominated by a single root

$$\frac{\partial^2 \vec{u}}{\partial t^2} = -\frac{\lambda}{\beta}\left(\frac{\mathrm{Im}(\Theta)\sigma}{\omega} + \mathrm{Re}(\Theta)\right)\vec{u} + \left(\frac{\lambda}{\beta}\frac{\mathrm{Im}(\Theta)}{\omega} - (1-\phi_o)\eta\lambda - k^2\eta\right)\frac{\partial \vec{u}}{\partial t} \tag{B36}$$

which can be expressed in terms of σ and ω using the relations (B17c) and (B18)

$$\frac{\partial^2 \vec{u}}{\partial t^2} = -(\sigma^2+\omega^2)\vec{u} + 2\sigma\frac{\partial \vec{u}}{\partial t} \tag{B37}$$

which is similar to the evolution equation of an harmonic oscillator under a linear drag (if $\sigma < 0$), or propelling (if $\sigma > 0$) force. We define a potential Φ similar to the elastic potential of an harmonic oscillator, and a kinetic energy K to be

$$\Phi = \frac{1}{2}u^2(\sigma^2+\omega^2), \qquad K = \frac{1}{2}\frac{\partial \vec{u}}{\partial t}\cdot\frac{\partial \vec{u}}{\partial t} \tag{B38}$$

where $u^2 = u_x^2 + u_y^2$. An 'energy' $\mathcal{E}$ can then be defined as the sum of the kinetic energy and the potential

$$\mathcal{E} \equiv \Phi + K \tag{B39}$$

Multiplying both side the above equation by the velocity $\frac{\partial \vec{u}}{\partial t}$ leads to

$$\frac{\partial}{\partial t}\left(\frac{1}{2}\frac{\partial \vec{u}}{\partial t}\cdot\frac{\partial \vec{u}}{\partial t}\right) = -\frac{\partial}{\partial t}\left(\frac{1}{2}(\sigma^2+\omega^2)\vec{u}\cdot\vec{u}\right) + 4\sigma\left(\frac{1}{2}\frac{\partial \vec{u}}{\partial t}\cdot\frac{\partial \vec{u}}{\partial t}\right) \tag{B40}$$

which according to the definitions in eqs (B38) and (B39), becomes

$$\frac{\partial \mathcal{E}}{\partial t} = 4\sigma K \tag{B41}$$

We can further identify the contribution by the three forces to $\partial \mathcal{E}/'\partial t$ by substituting eqs (B18) back to (B41):

$$\begin{aligned}\frac{\partial \mathcal{E}}{\partial t} &= \frac{2\lambda}{\beta}\frac{\mathrm{Im}(\Theta)}{\omega}K - 2(1-\phi_o)\eta\lambda K - 2k^2\eta K \\ &= \quad \mathcal{W}^g \quad + \quad \mathcal{W}^{\mathrm{ad}} \quad + \quad \mathcal{W}^{\mathrm{vb}}\end{aligned} \tag{B42}$$

where $\mathcal{W}^{\mathrm{ad}}$, $\mathcal{W}^{\mathrm{vb}}$ and $\mathcal{W}^g$ are defined as the power sources provided by the three corresponding forces

$$\mathcal{W}^{\mathrm{vb}} = -2k^2\eta K \qquad \mathcal{W}^{\mathrm{ad}} = -2(1-\phi_o)\eta\lambda K \qquad \mathcal{W}^g = \frac{2\lambda}{\beta}\frac{\mathrm{Im}(\Theta)}{\omega}K \tag{B43}$$

among which $\mathcal{W}^g$ indicates the rate of work done by the gas pressure force, and is referred to as the Bernoulli power source when the Bernoulli perturbation dominates. The total power source (i.e. the rate of works done by all forces) to the system is

$$\mathcal{W}^{\mathrm{tot}} = 2\left(-k^2\eta - (1-\phi_o)\eta\lambda + \frac{\lambda}{\beta}\frac{\mathrm{Im}(\Theta)}{\omega}\right)K = 4\sigma K \tag{B44}$$

Comparing eqs (B43) with (B32), we can observe that

$$\frac{\mathcal{W}^{\mathrm{ad,\,vb},g}}{2K} = \frac{\vec{\mathcal{T}}^{\mathrm{ad,vb},g}}{\vec{L}}$$

Therefore, the rates of work done by different forces varies with k and s in the same way as the torques. Similar to the angular momentum, the total rate of work done to the system is positive when the Bernoulli perturbation dominates.

APPENDIX C: NON-LINEAR EFFECTS OF LARGE COLUMN DISPLACEMENT

C1 Non-linear damping of the angular momentum and energy

When the magnitude of the column displacement u increases due to the unstable root, the non-linear effects become important in the system when the approximation of $O(u^2) = 0$ no longer satisfies. Especially, as u approaches the annulus' width ($u \to 1$), the most deformed annulus section becomes infinitely thin, and the shear stress at the column–annulus interface, hence the annulus drag force $\vec{F}^{\mathrm{ad}}$, approaches infinity. Because $\vec{F}^g$ and $\vec{F}^{\mathrm{vb}}$ remain finite at large displacement, the strong increase in $\vec{F}^{\mathrm{ad}}$ can drastically decrease the energy and angular momentum once the non-linear damping effect of $\vec{F}^{\mathrm{ad}}$ becomes larger than the Bernoulli effect in $\vec{F}^g$. As shown in Appendix B5, $\vec{L}$ and $\mathcal{E}$ grow with time at small displacement, before they are damped out by the non-linear drag force. This indicates that a transition must happen at a critical displacement where the total torque and rate of work changes from being positive to negative due the increased importance of the non-linear damping effect.

The non-linear annulus drag force $\vec{F}^{\mathrm{ad}}$, derived in Appendix A2 is expressed by its radial and tangential components in eq. (A16) in polar-cylindrical coordinates

$$F_u^{\mathrm{ad}} = \hat{u}\cdot\vec{F}^{\mathrm{ad}}, \qquad F_\psi^{\mathrm{ad}} = \hat{z}\cdot\left(\hat{u}\times\vec{F}^{\mathrm{ad}}\right) \tag{C1}$$

where $\hat{u}$ is the radial basis $\hat{u} = \vec{u}/u$. We use the same scales in Appendix B1 to non-dimensionlaize the force, where the length scale is the annulus' thickness $R_c - R_m$, velocity scale is the isothermal gas sound speed C_g and timescale is $(R_c - R_m)/C_g$. The forces are non-dimensionalized by the product of the acceleration scale $\frac{C_g^2}{R_c - R_m}$ and the mass of a magma column section $\pi R_m^2 \rho_m \mathrm{d}z$. The dimensionless form of eq. (A16) becomes

$$F_u^{\mathrm{ad}} = -(\hat{u}\cdot\hat{v})\eta\zeta\lambda(1-\phi_o)v + 4(\hat{u}\cdot\hat{v})\eta\lambda^2(\zeta-1)(1-\phi_o)v\left(\frac{\frac{3\lambda+1}{2\lambda}}{1+\sqrt{1-u^2}} - \frac{3}{4}\right) \tag{C2a}$$

$$F_\psi^{\mathrm{ad}} = \hat{z}\cdot(\hat{u}\times\hat{v})\eta\zeta\lambda(1-\phi_o)v - 4\hat{z}\cdot(\hat{u}\times\hat{v})\eta\lambda^2(\zeta+1)(1-\phi_o)v\left(\frac{1}{4} - \frac{1}{\sqrt{1-u^2}}\left(1 - \frac{\frac{3\lambda+1}{2\lambda}}{1+\sqrt{1-u^2}}\right)\right) \tag{C2b}$$

where dimensionless numbers λ, η and ζ where defined in eqs (B2) and (B4). Comparing eqs (C1) and (C2b), we further expand the torque generated by the non-linear annulus drag force $\vec{\mathcal{T}}^{\mathrm{ad}} = \vec{u}\times\vec{F}^{\mathrm{ad}} = uF_\psi^{\mathrm{ad}}\hat{z}$ into

$$\vec{\mathcal{T}}^{\mathrm{ad}} = \eta\zeta\lambda(1-\phi_o)\vec{L} - 4\eta\lambda^2(\zeta+1)(1-\phi_o)\vec{L}\left(\frac{1}{4} - \frac{1}{\sqrt{1-u^2}}\left(1 - \frac{\frac{3\lambda+1}{2\lambda}}{1+\sqrt{1-u^2}}\right)\right) \tag{C3}$$

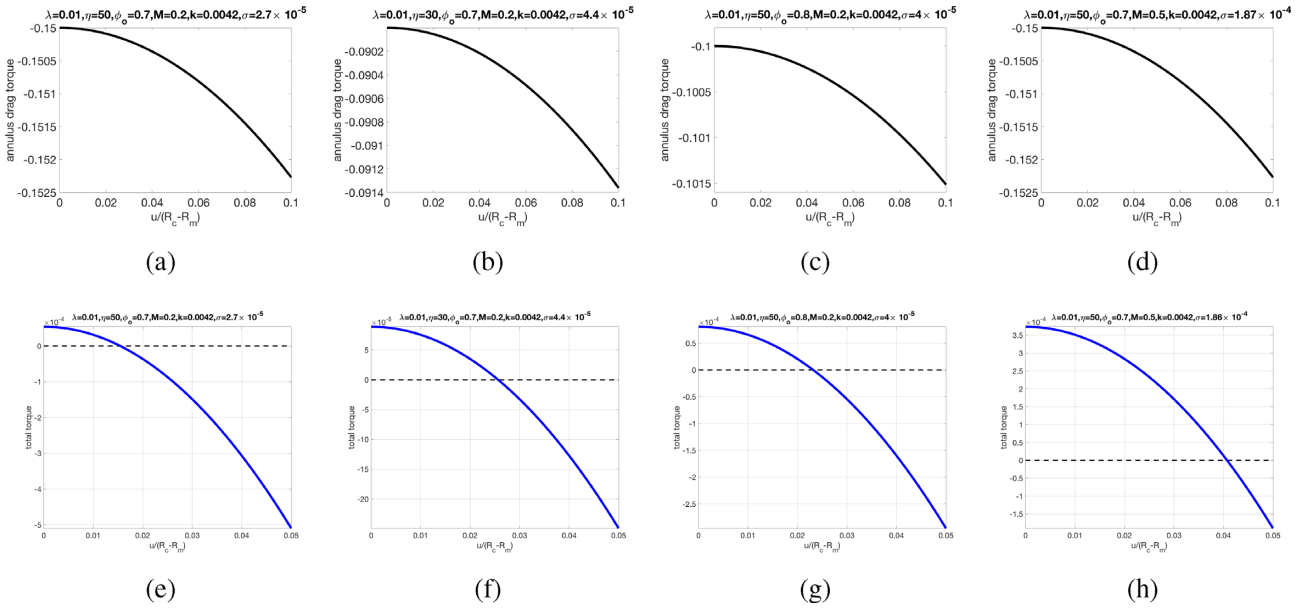

Figure C1. (a)–(d) show the non-linear annulus drag torque as function of the displacement magnitude. (e)–(h) show the total non-linear torque as function of the displacement magnitude. The function are shown with variations in system parameters M, λ, η and ϕ_o. The intersection of total torque with 0 (dash line) indicates the critical displacement u_c.

where the angular momentum $\vec{L} = \vec{u} \times \vec{v} = uv(\hat{u} \times \hat{v})$. Define

$$\Omega(u) = \frac{4\left(1+\frac{1}{\zeta}\right)}{\sqrt{1-u^2}} \frac{\frac{1+\lambda}{2\lambda} - \sqrt{1-u^2}}{1+\sqrt{1-u^2}} + 1 + \frac{1}{\zeta} \tag{C4}$$

the torque becomes

$$\vec{\mathcal{T}}^{\text{ad}} = \eta\zeta\lambda(1-\phi_o)\vec{L}\,(1-\lambda\Omega(u)) \tag{C5}$$

Note that $\Omega(u) > 0$ and monotonically increases with u. Therefore, the torque $\vec{\mathcal{T}}^{\text{ad}}$ always has the opposite sign with the angular momentum. When the displacement increases, $\vec{\mathcal{T}}^{\text{ad}}$ increases rapidly and is always opposite in sign to $\vec{L}$, hence the non-linear damping of the angular momentum becomes stronger (Figs C1 a–d). The instantaneous rate of work done by the non-linear annulus drag force $\mathcal{W}^{\text{ad}} = \vec{v} \cdot \vec{F}^{\text{ad}} = vF^{\text{ad}} \cos \angle^{\vec{F}^{\text{ad}}}_{\hat{v}}$. Using eq. (A5), we further express $\mathcal{W}^{\text{ad}}$ as

$$\begin{aligned}\mathcal{W}^{\text{ad}} &= vF^{\text{ad}} \cos\angle^{\hat{u}}_{\hat{v}} \cos\angle^{\vec{F}^{\text{ad}}}_{\hat{u}} - vF^{\text{ad}} \sin\angle^{\hat{u}}_{\hat{v}} \sin\angle^{\vec{F}^{\text{ad}}}_{\hat{u}} \\ &= \cos\angle^{\hat{u}}_{\hat{v}}(\hat{u}\cdot\vec{F}^{\text{ad}})v - \sin\angle^{\hat{u}}_{\hat{v}}\hat{z}\cdot\left(\hat{u}\times\vec{F}^{\text{ad}}\right)v \\ &= (\hat{u}\cdot\hat{v})vF^{\text{ad}}_u + \hat{z}\cdot(\hat{u}\times\hat{v})vF^{\text{ad}}_\psi\end{aligned} \tag{C6}$$

Substituting eqs (C2) into (C6), we obtain the rate of work done by the non-linear viscous drag force

$$\begin{aligned}\mathcal{W}^{\text{ad}} =& v^2\cos^2\psi^v_u\eta\lambda(1-\phi_o)\left(-\zeta+4\lambda(\zeta-1)\left(\frac{\frac{3\lambda+1}{2\lambda}}{1+\sqrt{1-u^2}}-\frac{3}{4}\right)\right) \\ &+ v^2\sin^2\psi^v_u\eta\lambda(1-\phi_o)\left(\zeta-4\lambda(\zeta+1)\left(\frac{1}{4}-\frac{1}{\sqrt{1-u^2}}\left(1-\frac{\frac{3\lambda+1}{2\lambda}}{1+\sqrt{1-u^2}}\right)\right)\right)\end{aligned} \tag{C7}$$

where $\psi^v_u = \angle^{\hat{v}}_{\hat{u}}$ is the angle between the displacement $\vec{u}$ and the velocity $\vec{v}$. We define another u-depended variable

$$\Psi(u) = -1 + 4\lambda\left(1-\frac{1}{\zeta}\right)\left(\frac{\frac{3\lambda+1}{2\lambda}}{1+\sqrt{1-u^2}}-\frac{3}{4}\right) \tag{C8}$$

which leads to

$$\mathcal{W}^{\text{ad}} = 2K\eta\lambda(1-\phi_o)\zeta\left(\cos^2\psi^v_u\Psi(u) + \sin^2\psi^v_u(1-\lambda\Omega(u))\right) \tag{C9}$$

where $\Omega(u)$ was defined in eq. (C4). When $\psi^v_u = 0$ or π, the motion of the magma column is 2-D, and $\mathcal{W}^{\text{ad}}$ is always finite. In this case, the non-linear viscous damping may not be large enough to cause the decrease in energy, due to the finite value of $\Psi(u)$. When the motion of the magma column is 3-D, thus $\psi^v_u \neq 0$ or π, the damping effect can be infinitely large as $u \to 1$, hence the total energy eventually

decreases as the work done by the drag force becomes large enough. Especially, when the wagging motion is near circular with $\psi_u^v = \pi/2$, $\mathcal{W}^{\rm ad} = 2K\eta\lambda(1-\phi_o)\zeta\,(1-\lambda\Omega(u))$, which is similar to eq. (C5), thus

$$\frac{\vec{\mathcal{T}}^{\rm ad}}{\vec{L}} = \frac{\mathcal{W}^{\rm ad}|_{\psi_u^v=\frac{\pi}{2}}}{2K}$$

It is worth noticing that when the displacement magnitude is small enough such that $O(u^2) \sim 0$,

$$\Omega \to (1+\frac{1}{\zeta})\frac{1}{\lambda}, \quad \Psi \to -\frac{1}{\zeta}$$

which lead eqs (C5) and (C9) to recover their linear forms in eqs (B32) and (B43), respectively. We can further approximate the evolutions of energy and angular momentum of the system at large column displacement by substituting the linear torque and power source done by the linear viscous annulus drag force by the non-linear counterparts using eqs (C5) and (C9). As the effect of gas force and viscous bending force remain finite, we assume that the non-linear contribution of the annulus drag force is much more prominent, hence keeping the linear forms of the other two forces. Under this approximation, the total torque and power source in eqs (B34) and (B44) become

$$\vec{\mathcal{T}}^{\rm tot} = \left(2\sigma + \lambda\eta(1-\phi_o) + \vec{\mathcal{T}}^{\rm ad}\right)\vec{L} \tag{C10a}$$

$$\mathcal{W}^{\rm tot} = \left(4\sigma + 2\lambda\eta(1-\phi_o) + \mathcal{W}^{\rm ad}\right)K \tag{C10b}$$

which, using eqs (C5) and (C9), can be further expressed in u

$$\frac{\vec{\mathcal{T}}^{\rm tot}}{\vec{L}} = 2\sigma + (1+\zeta)\lambda\eta(1-\phi_o) - \eta\lambda^2\zeta(1-\phi_o)\Omega(u) \tag{C11a}$$

$$\frac{\mathcal{W}^{\rm tot}}{2K} = 4\sigma + 2\eta\lambda(1-\phi_o)\left(1+\zeta\Psi(u)\cos^2\psi_u^v + \zeta(1-\lambda\Omega(u))\sin^2\psi_u^v\right) \tag{C11b}$$

As the angular momentum at large displacement amplitude is eventually damped by the non-linear annulus drag force, but increases when the displacement amplitude is small, we can define a critical displacement at which the angular momentum transitions from increasing to decreasing. Such transition happens when the total torque decreases to zero, hence $\vec{\mathcal{T}}^{\rm tot}(u_c) = 0$. The critical displacement u_c therefore can be obtained from eq. (C11a)

$$\Phi(u_c) = \frac{2\sigma + (1+\zeta)\lambda\eta(1-\phi_o)}{\zeta\eta\lambda^2(1-\phi_o)} \tag{C12}$$

Once when $u > u_c$, the total torque becomes negative and the angular momentum starts decreasing (Figs C1 e–h). Despite the variation of the critical displacement for different parameters in the system, the evolution of the total torque is qualitatively the same, crossing 0 from positive to negative as the displacement increases. If the Bernoulli perturbation corresponds to a circular trajectory (i.e. $\psi_u^v = \pi/2$ or $3\pi/2$), the decrease in the energy of the system also occurs when the displacement amplitude reaches u_c, at which point $\mathcal{W}^{\rm tot}(u_c) = \vec{\mathcal{T}}^{\rm tot}(u_c) = 0$. When the Bernoulli perturbation corresponds to elliptical trajectories, the decrease in energy is postponed. Furthermore, if the trajectory is 2-D (i.e. $\psi_u^v = 0$ or π), the total power source $\mathcal{W}^{\rm tot}$ could still have a positive value even at $u = 1$. Therefore, whether and when the energy of the system will be damped by the non-linear drag force sensitively depends on the shape of the wagging trajectory.